Aberrant Function of the C-Terminal Tail of HIST1H1E Accelerates Cellular Senescence and Causes Premature Aging

Elisabetta Flex,[1,13,36] Simone Martinelli,[1,36] Anke Van Dijck,[2,3,36] Andrea Ciolfi,[4] Serena Cecchetti,[5] Elisa Coluzzi,[6] Luca Pannone,[1,4] Cristina Andreoli,[7] Francesca Clementina Radio,[4] Simone Pizzi,[4] Giovanna Carpentieri,[1,4] Alessandro Bruselles,[1] Giuseppina Catanzaro,[8] Lucia Pedace,[9] Evelina Miele,[9] Elena Carcarino,[9,33] Xiaoyan Ge,[10,34] Chieko Chijiwa,[11] M.E. Suzanne Lewis,[11] Marije Meuwissen,[2] Sandra Kenis,[3] Nathalie Van der Aa,[2] Austin Larson,[12] Kathleen Brown,[12] Melissa P. Wasserstein,[13] Brian G. Skotko,[14,15] Amber Begtrup,[16] Richard Person,[16] Maria Karayiorgou,[17] J. Louw Roos,[18] Koen L. Van Gassen,[19] Marije Koopmans,[19] Emilia K. Bijlsma,[20] Gijs W.E. Santen,[20] Daniela Q.C.M. Barge-Schaapveld,[20] Claudia A.L. Ruivenkamp,[20] Mariette J.V. Hoffer,[20] Seema R. Lalani,[10] Haley Streff,[10] William J. Craigen,[10] Brett H. Graham,[10,21] Annette P.M. van den Elzen,[22] Daan J. Kamphuis,[23] Katrin Õunap,[24,25] Karit Reinson,[24,25] Sander Pajusalu,[24,25,26] Monica H. Wojcik,[27] Clara Viberti,[28,29] Cornelia Di Gaetano,[28,29] Enrico Bertini,[4] Simona Petrucci,[30,31] Alessandro De Luca,[31] Rossella Rota,[9] Elisabetta Ferretti,[8,32] Giuseppe Matullo,[28,29] Bruno Dallapiccola,[4] Antonella Sgura,[6] Magdalena Walkiewicz,[10,35] R. Frank Kooy,[2,37,*] and Marco Tartaglia[4,37,*]

Histones mediate dynamic packaging of nuclear DNA in chromatin, a process that is precisely controlled to guarantee efficient compaction of the genome and proper chromosomal segregation during cell division and to accomplish DNA replication, transcription, and repair. Due to the important structural and regulatory roles played by histones, it is not surprising that histone functional dysregulation or aberrant levels of histones can have severe consequences for multiple cellular processes and ultimately might affect development or contribute to cell transformation. Recently, germline frameshift mutations involving the C-terminal tail of HIST1H1E, which is a widely expressed member of the linker histone family and facilitates higher-order chromatin folding, have been causally linked to an as-yet poorly defined syndrome that includes intellectual disability. We report that these mutations result in stable proteins that reside in the nucleus, bind to chromatin, disrupt proper compaction of DNA, and are associated with a specific methylation pattern. Cells expressing these mutant proteins have a dramatically reduced proliferation rate and competence, hardly enter into the S phase, and undergo accelerated senescence. Remarkably, clinical assessment of a relatively large cohort of subjects sharing these mutations revealed a premature aging phenotype as a previously unrecognized feature of the disorder. Our findings identify a direct link between aberrant chromatin remodeling, cellular senescence, and accelerated aging.

[1]Department of Oncology and Molecular Medicine, Istituto Superiore di Sanità, Rome, 00161 Italy; [2]Department of Medical Genetics, University of Antwerp, Edegem, 2650 Belgium; [3]Department of Neurology, Antwerp University Hospital, Edegem, 2650 Belgium; [4]Genetics and Rare Diseases Research Division, Ospedale Pediatrico Bambino Gesù, Istituto di Ricovero e Cura a Carattere Scientifico (IRCCS), Rome, 00146 Italy; [5]Microscopy Area, Core Facilities, Istituto Superiore di Sanità, Rome, 00161 Italy; [6]Department of Science, University Roma Tre, Rome, 00146 Italy; [7]Department of Environment and Health, Istituto Superiore di Sanità, Rome, 00161 Italy; [8]Department of Experimental Medicine, Sapienza University, Rome, 00161 Italy; [9]Department of Pediatric Onco-Hematology and Cell and Gene Therapy, Ospedale Pediatrico Bambino Gesù, IRCCS, Rome, 00146 Italy; [10]Department of Molecular and Human Genetics, Baylor College of Medicine, Houston, TX 77030, USA; [11]Department of Medical Genetics, University of British Columbia, Vancouver, British Columbia V6H 3N1, Canada; [12]Section of Clinical Genetics and Metabolism, Department of Pediatrics, University of Colorado School of Medicine, Aurora, CO 80045, USA; [13]Children's Hospital at Montefiore, Albert Einstein College of Medicine, Bronx, NY 10467, USA; [14]Division of Medical Genetics and Metabolism, Department of Pediatrics, Massachusetts General Hospital, Harvard Medical School, Boston, MA 02114, USA; [15]Department of Pediatrics, Harvard Medical School, Boston, MA 02114, USA; [16]GeneDx, Gaithersburg, MD 20877, USA; [17]Department of Psychiatry, Columbia University Medical Center, New York, NY 10032, USA; [18]Department of Psychiatry, University of Pretoria, Weskoppies Hospital, Pretoria, 0001 South Africa; [19]Department of Genetics, Center for Molecular Medicine, University Medical Center Utrecht, Utrecht University, Utrecht, 3508 AB the Netherlands; [20]Department of Clinical Genetics, Leiden University Medical Center, Leiden, 2300 RC the Netherlands; [21]Department of Medical and Molecular Genetics, Indiana University School of Medicine, Indianapolis, IN 46202, USA; [22]Departement of Pediatrics, Reinier de Graaf Ziekenhuis, Delft, 2600 GA the Netherlands; [23]Departement of Neurology, Reinier de Graaf Ziekenhuis, Delft, 2600 GA the Netherlands; [24]Department of Clinical Genetics, United Laboratories, Tartu University Hospital, Tartu, 50406 Estonia; [25]Institute of Clinical Medicine, University of Tartu, Tartu, 50406 Estonia; [26]Department of Genetics, Yale University School of Medicine, New Haven, CT 06510, USA; [27]Broad Institute of MIT and Harvard, Cambridge, MA 02142, USA; [28]Department of Medical Sciences, University of Turin, Turin, 10126 Italy; [29]Italian Institute for Genomic Medicine, Turin, 10126 Italy; [30]Department of Clinical and Molecular Medicine, Sapienza University, Rome, 00189 Italy; [31]Division of Medical Genetics, Casa Sollievo della Sofferenza Hospital, IRCCS, San Giovanni Rotondo, 71013 Italy; [32]Istituto Neuromed, IRCCS, Pozzilli, 86077 Italy; [33]Current affiliation: Cordeliers Research Centre, Inserm 1138, Sorbonne Université, Paris, 75006 France; [34]Current affiliation: Department of Genetics and Genomic Sciences, The Icahn School of Medicine at Mount Sinai, New York, NY 10029, USA; [35]Current affiliation: National Institute of Allergy and Infectious Disease, National Institutes of Health, Bethesda, MD 20892, USA
[36]These authors contributed equally to this work
[37]These authors contributed equally this work
*Correspondence: frank.kooy@uantwerpen.be (R.F.K.), marco.tartaglia@opbg.net (M.T.)
https://doi.org/10.1016/j.ajhg.2019.07.007.

Introduction

In eukaryotic cells, nuclear DNA is organized in a complex and dynamic structure called chromatin, which allows efficient packaging of the genome and proper chromosomal segregation during mitosis; chromatin also controls the genome's accessibility for essential processes such as replication, transcription, and repair.[1] The basic unit of chromatin is the nucleosome, in which a stretch of about 147 bp of DNA wraps around an octamer of the core histones (i.e., H2A, H2B, H3, and H4), constituting the nucleosomal core particle (NCP).[2] A number of H1 linker histone isoforms bind to short DNA segments at the entry and exit sites on the surface of the NCP, stabilizing the nucleosomal structure and contributing to higher-order chromatin folding.[3,4] Although H1 histones have traditionally been associated with chromatin compaction and a regulatory function favoring transcriptional repression,[5] a more complex and plastic role of these proteins in the control of accessibility to DNA has gradually been appreciated.[6–8] In mammals, H1 histones are encoded by 11 genes. Among these, seven are expressed in somatic cells, and the remaining four are transcriptionally active in the germline.[3,4] Of note, even among the seven somatic subtypes, the levels of these proteins appear to be regulated during the cell cycle and development, and in different tissues and cell types, suggesting specific functions for individual isoforms.[9] On the other hand, redundancy in their function has been reported.[10,11] In higher eukaryotes, H1 histone isoforms share a tripartite structure consisting of a central highly conserved globular domain and two less-conserved, unstructured N-terminal and C-terminal tails. The globular domain has high sequence homology among H1 subtypes and mediates binding to the nucleosome. The two tails are moderately conserved among orthologs but differ among isoforms, suggesting functional specificity. Notably, both tails encompass a number of residues that are subjected to reversible modifications with regulatory function. Among these, the extent of phosphorylation in serine/threonine residues at the C-terminal tail has been proposed to regulate chromatin dynamics in interphase as well as chromosome condensation during mitosis.[4,12]

Aberrant histone function, whether due to mutations in genes coding proteins that participate in histone-modifying complexes or mutations directly affecting histone-coding genes, has been established as contributing to oncogenesis and causing multisystem syndromes that affect growth and cognitive function.[13–18] Recently, germline frameshift mutations affecting *HIST1H1E* (MIM: 142220), which codes a member of the somatic, replication-dependent linker histone subfamily, have been causally linked to an as-yet poorly defined syndrome that includes intellectual disability (ID) (MIM: 617537).[19] Mutations were mapped at the C-terminal tail of HIST1H1E and were predicted to have an equivalent functional impact by generating the same change in the reading frame. The five affected individuals belonged to a cohort of subjects with overgrowth, and were reported to have a similar facial appearance but variable height, head circumference, and degree of ID.[19] Notably, the growth pattern of these individuals appeared to be complex and characterized by a height that was above average during infancy but that became progressively closer to average over time until it could be characterized as average or short in adulthood. This peculiar pattern of growth has been highlighted by a subsequent report, which also confirmed the association of this class of *HIST1H1E* mutations with ID and specific facial features.[20]

Here, we report that this homogeneous class of disease-causing frameshift mutations affecting the C-terminal tail of HIST1H1E results in stable proteins that reside in the nucleus and bind to chromatin but disrupt proper compaction of DNA and are associated with a specific methylation profile. We also provide data indicating that cells expressing these mutant proteins have a dramatically reduced proliferation rate and competence, hardly enter into the S phase, and undergo accelerated senescence. Remarkably, clinical assessment of 13 newly identified individuals who are heterozygous for this class of mutations and of those previously reported allowed us to identify premature aging as a previously unrecognized feature of the disorder. Collectively, these data highlight a strict link between aberrant chromatin remodeling, cellular senescence, and accelerated aging.

Material and Methods

Subjects

This study was approved by the Committee for Medical Ethics, University of Antwerp, Antwerp, and Ethical Committee, Ospedale Pediatrico Bambino Gesù, Rome. Clinical data and DNA specimens from the subjects included in this study were collected according to procedures conforming to the ethical standards of the declaration of Helsinki protocols and approved by the review boards of all involved institutions, and signed informed consent was obtained from the participating subjects and/or families. Explicit permission was obtained to publish the photographs of the subjects as shown in Figure 1.

Exome Sequencing

WES was performed with DNA samples obtained from leukocytes. In most cases, a trio-based strategy was used. Exome capture was carried out with the Nimblegen SeqCap EZ Exome v3 (Roche) (subjects 1 and 5), Clinical Research Exome (Agilent) (subjects 2 and 3), SeqCap EZ VCRome v2.1 (Roche) (subjects 6 and 7), SureSelect Human All Exon v4 (Agilent) (subjects 8, 9 and 13), SureSelect Human All Exon v5 (Agilent) (subjects 4 and 12), and SureSelect XT Human All Exon v6 (Agilent) (subjects 10 and 11) target enrichment kits, and sequencing was performed on HiSeq 2000/2500/4000 and NextSeq550 platforms (Illumina) through the use of paired-end reads. WES data processing, sequence alignment to GRCh37, and variant filtering and prioritization by allele frequency, predicted functional impact, and inheritance models were performed as previously described.[21–27] The *de novo* origin of the *HIST1H1E* frameshifts was confirmed by Sanger sequencing in all cases.

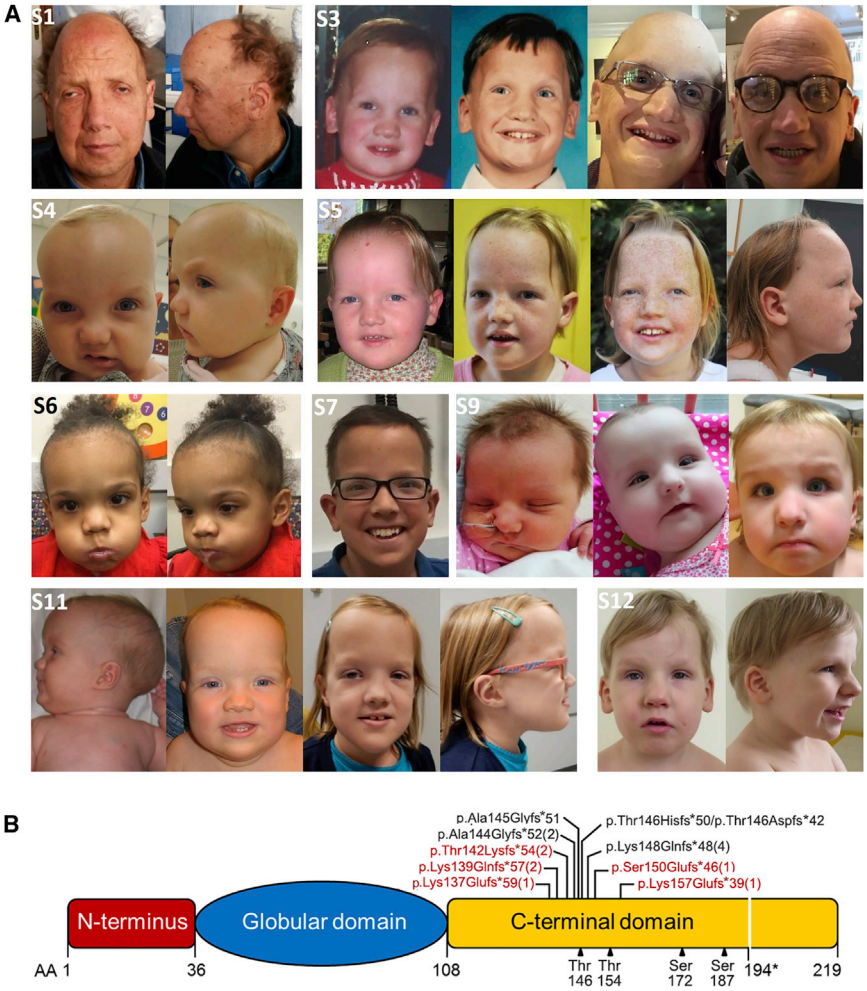

Figure 1. Facial Appearance of Subjects with *HIST1H1E* Frameshift Mutations and Protein Structure

(A) In affected individuals, facial appearance is characterized by a high anterior hairline, prominent forehead, bitemporal narrowing, sparse temporal hair, hypertelorism, hooded eyelids, short palpebral fissures, a high and broad nasal bridge, and a full nasal tip; small, widely spaced teeth; and low-set ears. A facial appearance compatible with a more advanced age (e.g., hypotrichosis and ptosis) is evident in S1 and S3. (S1, 49 years; S3, 30 years at last evaluation; S4, 14 months; S5, 12 years at last evaluation; S6, 3 years; S7, 12 years; S9, 2 years at last evaluation; S11, 6 years at last evaluation; and S12, 4 years)

(B) Schematic diagram representing the HIST1H1E structure, which is composed of a globular domain flanked by N- and C-terminal tails. The position of the disease-causing frameshift mutations is shown above the cartoon. (Novel mutations are highlighted in red.) The number of independent cases identified in the present study is in brackets. The domain boundaries and cyclin-dependent kinase phosphorylation sites (black triangles) are reported below the cartoon. All mutations are expected to result in a shorter protein with an identical divergent C-terminal tail. (The new stop codon is shown below the cartoon, 194.*)

RNA Stability

Total RNA was isolated from circulating leukocytes of subjects 1 and 2 (S1 and S2, hereafter) through the use of the RNeasyMiniKit (QIAGEN). Reverse transcription was performed with the SuperScriptIII first strand kit (Invitrogen) according to the manufacturer's instructions. Primer sequences used for RT-PCR are available upon request.

Constructs

The c.441dupC (p.Lys148Glnfs*48), c.464dupC (p.Lys157Glufs*39), and c.441_442insCC (p.Lys148Profs*82) were introduced by site-directed mutagenesis in a *HIST1H1E* cDNA (RefSeq: NM_005321.2, NP_005312.1) tagged with Xpress at the N terminus and cloned in pcDNA6/His version C (Invitrogen).

Cell Cultures and Transfections

Skin fibroblasts isolated from skin biopsies (subjects S1 and S2 and healthy donors), and COS-1 and HeLa lines were cultured in Dulbecco's modified Eagle's medium supplemented with 10% heat-inactivated fetal bovine serum (GIBCO) and 1% penicillin-streptomycin, at 37°C with 5% CO_2.

SCGE Assay

Samples were processed according to the alkaline single-cell gel electrophoresis (SCGE) assay protocol, as previously described.[28] In brief, cells were suspended in 0.7% low-melting agarose. Slides were prepared in duplicates with control cells and fibroblasts derived from affected individuals placed on opposite sides of the same slide, immersed in cold lysis solution, and kept at 4°C overnight. After lysis, slides were transferred in alkaline buffer for 20 min. Electrophoresis was carried out for 20 min at 20 V and 300 mA (0.8 V/cm) at 4°C. We explored the basal level of nucleoid relaxation by applying longer electrophoresis run times (40 and 60 min). Slides were neutralized in 0.4 M Tris (pH 7.5) for 5 min, treated with absolute ethanol, and stored at room temperature. Slides were then stained with GelRed (Biotium) and scored at a fluorescence microscope (Leica). To evaluate induced DNA damage and DNA repair capability, we irradiated fibroblasts with 1 or 2 Gy γ-rays from a 137Cs source at a dose rate of 0.8 Gy/min. During treatment, cells were maintained at 0°C so that DNA repair would be prevented. The kinetics of DNA repair were assessed by SCGE assay, as described above. The residual DNA damage was measured after 15 and 30 min of incubation at 37°C. For each experimental point, at least 75 cells were analyzed.

Histone Modifications and Nucleolus Morphology Assessment

For immunofluorescence, fibroblasts from S1 and control subjects were seeded at a density of 20×10^3 in 24-well cluster plates onto 12 mm cover glasses. After 24 h of culture in complete medium,

cells were fixed with 3% paraformaldehyde. Following permeabilization with 0.5% Triton X-100 (10 min at room temperature), fibroblasts were stained with anti-dimethyl-Histone H3 (lys4) rabbit polyclonal antibody, anti-trimethyl-histone H3 (lys9) rabbit polyclonal antibody, anti-trimethyl-histone H3 (lys27) rabbit polyclonal antibody (Millipore), and anti-heterochromatin protein-1β mouse monoclonal antibody (Chemicon) followed by the appropriate secondary antibody (Invitrogen) and DAPI. To study nucleolus morphology, we stained fibroblasts with C23 (MS-3) mouse monoclonal antibody (Santa Cruz) followed by the appropriate secondary antibodies (Invitrogen) and DAPI. Observations were performed on a Leica TCS SP2 AOBS apparatus. Cells stained only with the fluorochrome-conjugated secondary antibodies were used for setting up acquisition parameters. Signals from different fluorescent probes were taken in sequential scanning mode, several fields (>200) were analyzed for each labeling condition, and representative results are shown.

Proliferation and Cell-Cycle Assays

Cells were seeded at 200,000 cells per well in a 6-well plate and incubated a 37°C. Cell numbers (mean of three replicates ± SD) were counted by trypan blue exclusion after 4 and 7 days. The percentages of cells in different cell-cycle phases were determined by dual flow-cytometry analysis of BrdU-positive cells stained with the fluorescent DNA probe propidium iodide (PI). In brief, cells were incubated for 1 h with BrdU (Sigma Aldrich) at a final concentration of 30 μM. Then BrdU was removed, and cells were rinsed with PBS, harvested, and permeabilized in ice-cold 100% EtOH. Cells were incubated with HCl 3N to denature DNA and then with 0.1 M sodium tetraborate to stop this reaction. Fibroblasts were incubated with the anti-BrdU antibody (Invitrogen) followed by goat anti-mouse Alexa Fluor 488 secondary antibody. Finally, cells were resuspended in a buffer containing 10 μg/mL RNase A and 20 μg/mL PI and then immediately analyzed through the use of FACSCalibur (BD Biosciences).

SA-β-gal Activity and P53 Evaluation

SA-β-gal activity was assessed as reported.[29] In brief, cells were fixed with 3.6% formaldehyde in PBS for 4 min at room temperature. Fixed cells were washed and then incubated overnight with freshly prepared staining solution at 37°C in the absence of CO_2. After being washed, the coverslips were mounted with the antifade Dako fluorescence mounting medium (Agilent Technologies). P53 endogenous levels were evaluated on fibroblast lysates collected at different passages using an anti-p53 mouse monoclonal antibody (Invitrogen). Membranes were probed with an anti-GAPDH mouse monoclonal antibody (Santa Cruz) so that protein content would be normalized.

Analysis of Nuclear Morphology

After 24 h of culture in complete medium, fibroblasts were treated with 2 mM thymidine (Sigma) for 24 h, washed with 1× PBS, recovered with complete medium for 3 h, and then treated with 100 ng/mL nocodazole (Sigma) for 12 h. Afterward, fresh drug-free medium was added, and recovery was allowed for 120 min during which cells were fixed every 15 min in PHEMO buffer for 10 min at room temperature, as previously described.[30] Finally, cells were stained with lamin A/C mouse monoclonal antibody (Santa Cruz) followed by the appropriate secondary antibody (Invitrogen) and DAPI. Observations were performed on a Leica TCS SP2 AOBS apparatus as described above.

Evaluation of rRNA Content

Total RNA was extracted from the same amount of control fibroblasts and cells derived from affected individuals (400,000 fibroblasts) at different cellular passages. Three μL of total RNA was loaded for size separation on 1% agarose gel and stained with ethidium bromide.

Evaluation of Protein Stability

COS-1 cells were seeded in 6-well plates the day before transfection. Cells were transfected at 70% confluency with Fugene 6 transfection reagent (Promega) with wild-type or mutant Xpress-tagged *HIST1H1E* expression constructs. Forty-eight h after transfection, cells were treated with cycloheximide (20 μg/mL) for 8 and 16 h or left untreated before lysis. Immunoblotting was performed so that Xpress-tagged HIST1H1E levels could be assessed. Probing membranes with an anti-GAPDH antibody (Santa Cruz) allowed normalization of protein content.

CSK Assay

Twenty thousand fibroblasts and 30×10^3 HeLa cells were seeded on a glass coverslip and maintained in culture complete medium for 24 h. HeLa cells were transfected with 100 ng of vectors expressing Xpress-tagged HIST1H1E. Forty-eight h after transfection, HeLa cells were either fixed with 3% paraformaldehyde or treated with CSK buffer before being fixed.[31] After permeabilization with 0.5% Triton X-100 (for 10 min at room temperature), HeLa cells were stained with monoclonal antibody to Xpress (Invitrogen) and then with the appropriate secondary antibody (Invitrogen) and DAPI for DNA. Analyses were performed in three independent experiments on a Leica TCS SP2 AOBS apparatus.

Analysis of Cell Morphology

Fibroblasts from subject S1 and a control individual were seeded in a 100 mm dish cell culture. Optical microscope images at different passages were taken with Floid Cell Imaging Station (Life Technologies).

γH2AX Immunofluorescence Staining

Cells were seeded on a glass in a Petri dish for 24 h. The slides were fixed with 4% paraformaldehyde (Sigma Aldrich), permeabilized in 0.2% Triton X-100, and blocked in PBS/BSA 1% for 30 min at room temperature. Slides were incubated with a mouse monoclonal anti-phospho-histone H2AX antibody (Millipore) overnight at 4°C, washed in PBS/BSA 1%, and then exposed to the secondary Alexa 488-labeled donkey anti-mouse antibody (Invitrogen, Life Technologies) for 1 h at 37°C. After washes in PBS/BSA, 1% DNA were counterstained with DAPI (Sigma Aldrich) in Vectashield (Vector Laboratories). Cells were analyzed with fluorescence microscopy using an Axio Imager Z2 microscope (Zeiss). The frequency of foci per cell was scored in 150 nuclei in two independent experiments.

Telomere Dysfunction-Induced Foci (TIF) ImmunoFISH Staining

Cells were seeded on glass slides that were processed as reported for the γH2AX immunofluorescence staining up to the secondary antibody (Alexa 488-labeled donkey anti-mouse, Invitrogen). Immediately after, slides were washed in PBS/Triton X-100 0.05%, fixed in 4% formaldehyde for 2 min and dehydrated through graded alcohols (70%, 80%, and 100%). Slides and probes (Cy3 linked telomeric PNA probe, DAKO) were co-denatured at

80°C for 3 min and hybridized for 2 h at room temperature in a humidified chamber. After hybridization, slides were washed twice for 15 min in 50% formamide, 10 mM Tris, pH 7.2, and 0.1% BSA followed by three 5-min washes in 0.1 M Tris, pH 7.5; 0.15 M NaCl; and 0.08% Tween 20. Slides were then dehydrated with an ethanol series and air dried. Finally, slides were counterstained with DAPI (Sigma Aldrich) in Vectashield (Vector Laboratories). Co-localization between γH2AX foci and telomere were analyzed using an Axio Imager Z2 microscope (Zeiss). The frequency of co-localization dots per cell was scored in 150 nuclei in two independent experiments.

Quantitative-Fluorescence *In Situ* Hybridization Analysis (Q-FISH)

Chromosome spreads were obtained as reported above. Q-FISH staining was performed as previously described,[32] with minor modifications. In brief, slides and probes (Cy3 linked telomeric, PANAGENE, and chromosome 2 centromeric PNA probes, DAKO) were co-denatured at 80°C for 3 min and hybridized for 2 h at room temperature in a humidified chamber. Slides were counterstained with DAPI (Sigma Aldrich) in Vectashield (Vector Laboratories). Images were captured at a 63X magnification with an Axio Imager Z2 (Zeiss). ISIS software (MetaSystems) was used to assess telomere size (defined as ratio between total telomeres' fluorescence [T] and fluorescence of the centromeres of the two chromosomes 2 [C]). Data were expressed as T/C %.[33] Experiments were repeated two times and at least 10–15 metaphases were scored each time.

Detection of Aneuploidy

Chromosome spreads were obtained as described before. Metaphases were captured at 63× magnification using an Axio Imager Z2 microscope (Zeiss). We considered euploidy to be the metaphases with 46 chromosomes and aneuploidy to be all of the metaphases that had a different number of chromosomes. The frequency of aneuploidy was scored in 40 metaphases. Two independent experiments were performed.

Chromosome Condensation Assay

After 30 min incubation with 30 μM Calyculin-A (Wako), a 28 min incubation at 37°C with hypotonic solution (75 mM KCl), and fixation in freshly prepared Carnoy solution (3:1 v/v methanol/acetic acid), chromosome spreads were obtained. Slides were stained with DAPI (Sigma Aldrich) in Vectashield (Vector Laboratories), and an Axio Imager Z2 microscope (Zeiss) was used. To analyze the frequency of chromosomal condensation, we counted the number of metaphases in 150 nuclei per sample in two independent experiments.

Methylome Profiling

We assessed the DNA methylation levels of one adult and five pediatric affected individuals through the use of the Infinium Human Methylation EPIC BeadChip assay (Illumina), which allows comprehensive genome-wide coverage, and genomic DNA extracted from leukocytes. Methylation levels were measured as beta values, percentages of methylation at each CpG site, and ranged from 0 (i.e., no methylation) to 1 (full methylation). Raw data were processed with the bioconductor package ChAMP[34] and the default parameters were used for filtering low-quality signals and normalizing data. Methylation profiles were compared with those obtained from a series of 35 healthy adult male controls of European descent; these included 31 individuals selected from a European cohort study (average age ± SD: 56.1 ± 7.4 years).[35] Unsupervised multidimensional scaling (MDS) analysis was used, and the 1,000 most variable probes among samples were taken into account. Statistical analyses were conducted with R software (v. 3.5.0). We performed gene and pathway enrichment analyses of the differentially methylated probes by using the Gene SeT AnaLysis online tool[36] on the associated genes. Functional annotation was carried out by means of GO terms including biological processes, molecular functions, and cellular components classes. Pathway analysis was performed using KEGG. Statistical significance was assumed at 0.05 following multiple testing adjustment (FDR).

Results

Spectrum of *HIST1H1E* Mutations and Associated Clinical Features

Using whole-exome sequencing (WES), we identified a novel *de novo HIST1H1E* frameshift variant, c.441dupC (p.Lys148Glnfs*48), in an adult individual with hypotrichosis, cutis laxa, and ID (S1) (Figure 1A). Mutation analysis performed on primary skin fibroblasts and hair bulb epithelial cells from the affected individual supported our hypothesis of a germline origin of the frameshift. The variant had not been reported in ExAC/gnomAD, and this variant affected a relatively large and highly conserved portion of the encoded protein. In the subject, WES data analysis excluded the presence of other functionally relevant variants compatible with known Mendelian conditions on the basis of the expected inheritance model and clinical presentation. Through networking and a GeneMatcher search,[37] we identified 12 additional individuals with similar *de novo* frameshift *HIST1H1E* mutations (Figure 1B, Table 1). All changes were short out-of-frame indels resulting in almost identical shorter proteins that contained a shared divergent C-terminal tail (Table S1); these results were consistent with previous reports.[19,20,38,39] None of the frameshifts had been reported in gnomAD, all were predicted to dramatically impact protein function, and two of them had already been reported in ClinVar as disease-causing mutations (Table 1).

We analyzed the clinical records of the 13 identified subjects (S1 to S13) and collected the information available for the seven previously published individuals (S14 to S20). All subjects had variable developmental delay (DD)/ID and a distinctive facies characterized by bitemporal narrowing (in 100% of individuals), a prominent forehead (93%), and a high anterior hairline (88%) as main features, which were reminiscent of Pallister-Killian syndrome (MIM: 601803) (Figure 1A). In four children, Sotos syndrome (MIM: 117550) had been suggested, and Weaver syndrome (MIM: 277590), Simpson-Golabi-Behmel syndrome (MIM: 312870), and Pallister-Killian syndrome had been suspected in single cases (Table S2). Half of the individuals had scaphocephaly and sparse frontotemporal hair. The

Table 1. Frameshift *HIST1H1E* Mutations Identified in This Study

Nucleotide Change[a]	gnomAD	ClinVar	Amino Acid Change	Domain	CADD[b]	Number of Cases	Origin
c.408dupG	-	-	p.Lys137Glufs*59	C-terminal tail	34	1	*de novo*
c.414dupC	-	-	p.Lys139Glnfs*57	C-terminal tail	35	2	*de novo* (1)
c.425_431delinsAGGGGGTT	-	-	p.Thr142Lysfs*54	C-terminal tail	31	1	*de novo*
c.425delinsAG	-	-	p.Thr142Lysfs*54	C-terminal tail	29	1	undetermined
c.430dupG	-	reported	p.Ala144Glyfs*52	C-terminal tail	26.8	2	undetermined
c.441dupC	-	reported	p.Lys148Glnfs*48	C-terminal tail	34	4	*de novo*
c.447dupG	-	-	p.Ser150Glufs*46	C-terminal tail	34	1	*de novo*
c.464dupC	-	-	p.Lys157Glufs*39	C-terminal tail	35	1	*de novo*

Nucleotide numbering reflects cDNA numbering with 1 corresponding to the A of the ATG translation initiation codon in the *HIST1H1E* reference sequence (RefSeq: NM_005321.2, NP_005312.1).
[a]ClinVar submission IDs: c.408dupG, SCV000925231; c.414dupC, SCV000925232; c.425_431delinsAGGGGGTT, SCV000925233; c.425delinsAG, SCV000925234; c.430dupG, SCV000925235; c.441dupC, SCV000925236; c.447dupG, SCV000925237; and c.464dupC, SCV000925238.
[b]CADD v1.4.

craniofacial appearance was characterized by hypertelorism (91%), downslanted palpebral fissures (67%), a broad nasal tip (83%), and low-set and posteriorly rotated ears (57%). Forty-three percent of subjects showed small, widely spaced teeth. Skin hyperpigmentation was present in one-third of individuals. Neonatal problems included hypotonia, feeding difficulties, failure to thrive, jaundice, congenital hypothyroidism, and micrognathia. Three individuals showed single palmar creases possibly related to prenatal hypotonia. Finger abnormalities included short fourth metacarpals, camptodactyly, fifth finger clinodactyly, brachydactyly, and broad and low-set thumbs. Toe abnormalities included long halluces, broad toes, and fifth toes overlapping fourth toes. Two individuals had pectus excavatum. Growth parameters at birth were unremarkable. At last evaluation, only one subject (S10) had macrosomy (>3.65 SD), and 12 individuals (63%) had a large head circumference (>+2.0 SD), including two children with relative macrocephaly at the age of 4 years. DD was present in all individuals. They were mildly to moderately intellectually disabled. Fourteen individuals had speech delay, and gross motor delay was a common feature. In young individuals, hypotonia and a stiff, clumsy, and uncoordinated gait were relatively common findings. The 49-year-old individual (S1) had gait ataxia. Behavioral features included ADHD (two individuals), autistic features (five individuals), and psychotic episodes (one individual). One child had focal seizures in early childhood, and another child was treated for recurrent status epilepticus. Brain MRI revealed aspecific abnormalities, including mild inferior vermian hypoplasia, delayed myelination, partial agenesis of the corpus callosum, and mild to moderately enlarged third and lateral ventricles. Five individuals presented with mild hearing loss. Visual problems included hypermetropia, myopia, astigmatism, and strabismus. Sixty percent of the individuals had feeding or eating difficulties, ranging from satiety problems at younger ages to problems with swallowing fluids or learning to eat solid food. One child was fed by G-tube at the age of 2.5 years. She had gastro-esophageal reflux disease and rumination disorder. Other remarkable features in this cohort included pancytopenia accompanying systemic lupus erythematosus in the oldest individual. A summary of the major features is reported in Table 2, and a more detailed description for each subject is available in Table S2.

Notably, the oldest individuals of the present cohort (S1 and S3) and two previously reported subjects (S15 and S17) had facial appearances compatible with a much more advanced age. When we evaluated the clinical presentation of the entire cohort of affected individuals, including those previously reported, we noticed an overrepresentation of features that are generally less common for individuals in this age group but more commonly found in elderly individuals. These features included hypotrichosis, ptosis, cutis laxa, hyperkeratosis, skin hyperpigmentation, dry skin, nail abnormalities, hearing loss, cataracts, diabetes mellitus, and osteopenia (Table S3). One girl was diagnosed with childhood hypophosphatasia (osteopenia and advanced bone age that was investigated after she presented with multiple small stress fractures of the lower limbs). Three other children also had advanced bone age. A fifth child had multiple fractures after minor trauma. Several children had dental problems including missing permanent teeth and small, fragile teeth.

Functional Characterization of *HIST1H1E* Mutations

Based on the unique narrow spectrum of mutations, we hypothesized a specific disruptive impact on HIST1H1E function as a consequence of the frameshift. Haploinsufficiency was considered unlikely because endogenous *HIST1H1E* mRNA levels from two unrelated affected subjects (S1, aged 49 years, and S2, aged 4 years) were comparable to those of controls, and transient transfection experiments involving Xpress-tagged *HIST1H1E* constructs in COS-1 cells documented an increased stability of the mutant proteins compared to the wild-type protein

Table 2. Summary of the Clinical Features Occurring in Subjects Carrying *de novo HIST1H1E* Frameshift Mutations

Clinical Features	Frequency[a]
DD/ID	**18/18[b] (100%)**
motor delay	12/12 (100%)
walking independently, range (mean), months	15–66 (31)
speech delay	14/14 (100%)
hypotonia	11/15 (73%)
autistic features	5/14 (36%)
Craniofacial Features	**19/19 (100%)**
macrocephaly	12/19 (63%)
scaphocephaly	6/11 (54%)
sparse hair	6/12 (50%)
high anterior hairline	14/16 (87%)
prominent forehead	13/14 (93%)
hypertelorism	10/11 (91%)
downslanted palpebral fissures	8/12 (67%)
full nasal tip	10/12 (83%)
low set ears	8/14 (57%)
Aging Appearence	**20/20 (100%)**
skin hyperpigmentation	5/15 (33%)
hypotrichosis	6/20 (30%)
skin hyperpigmentation	5/20 (25%)
nail abnormalities	6/20 (30%)
dental problems	6/20 (30%)
advanced bone age	4/20 (20%)
Other	**9/15 (60%)**
feeding or eating difficulties	9/15 (60%)
hearing loss	5/14 (36%)
strabismus	8/15 (53%)

[a]The reported cohort includes 13 presently described subjects and seven previously reported cases.
[b]Subjects showed variable ID: five mild, nine moderate, and two severe. In two cases, the severity of ID was unspecified.

(Figure S1). Furthermore, confocal microscopy analysis performed in transiently transfected HeLa cells showed proper nuclear localization and stable binding to chromatin of the tested mutants (Figure S2). These data, along with the finding that a mutant allele expressing the third open reading frame at an equivalent position of the C terminus (this allele does not occur in affected individuals) was characterized by compromised chromatin binding, indicating loss of function (Figure S2), strongly suggested a dominant negative or neomorphic effect as the mechanism of disease.

H1 linker histones are core chromatin components, and they bind to short DNA segments at the entry and exit sites on the surfaces of nucleosomes, stabilizing their structure and regulating chromatin folding.[4] The C-terminal tail of H1 histones contains a number of serine/threonine residues that undergo reversible phosphorylation, modulating the dynamics of chromatin compaction; these residues are lost in disease-associated HIST1H1E mutants. Of note, although partial phosphorylation of the C-terminal tail allows chromatin relaxation during interphase, full phosphorylation is required for maximal chromatin condensation during mitosis.[4,12] To assess chromatin compaction, we performed a single-cell gel electrophoresis (SCGE) assay in primary fibroblasts from subjects S1 and S2. Increasing run times allowed DNA loops to extend under the electrophoretic field and showed significantly more nucleoid relaxation in fibroblasts from affected individuals than in control cells; these results were quantified as "tail moment" values (Figure 2A). Because chromatin compaction is associated with a specific pattern of histone modifications, including methylation of histone H3 at specific lysine residues,[40] the methylation profile of histone H3 was assessed in the two fibroblast lines. Consistent with the SCGE data, a decrease in H3K4me2, H3K9me3, and H3K27me3 staining was documented by immunofluorescence analyses (Figure 2B). In line with these findings, reduced levels of HP1β, a member of the HP1 family mediating heterochromatinization by binding to methylated H3K9, and whose level is reduced in cells with a defective heterochromatin state,[41] was also observed (Figure 2C). Finally, a caliculin-induced premature chromosome condensation assay documented significantly fewer condensed chromosomes in fibroblasts from affected individuals (11.3% of analyzed cells) than in control cells (19.6%) ($p < 0.01$, χ^2 test). Overall, these data indicated a more relaxed state of chromatin in cells expressing the disease-causing HIST1H1E mutants.

Methylome Profiling

Because altered chromatin condensation is expected to impact DNA methylation,[42] we used a genome-wide methylation profiling analysis to investigate perturbations at the epigenome level. To this end, Infinium MethylationEPIC BeadChip profiling was used for comparing a subset of DNA samples obtained from leukocytes of six affected individuals to samples from a control group composed of 35 healthy individuals of European descent. When the entire set of assayed target probes is considered, the analysis did not highlight a substantial change in methylation pattern (data not shown). However, MDS analysis was carried out taking into account the information associated with the 1,000 most differentially methylated probes among all samples (independently from their group classification), and the results indicated clear-cut divergence between the methylation profiles of healthy controls and those of affected individuals, the latter clustering according to the ages of the individuals (Figure 2D). Among these informative probes, 170 differentially methylated CpGs were located within the UCSC CpG islands (from 200 bp

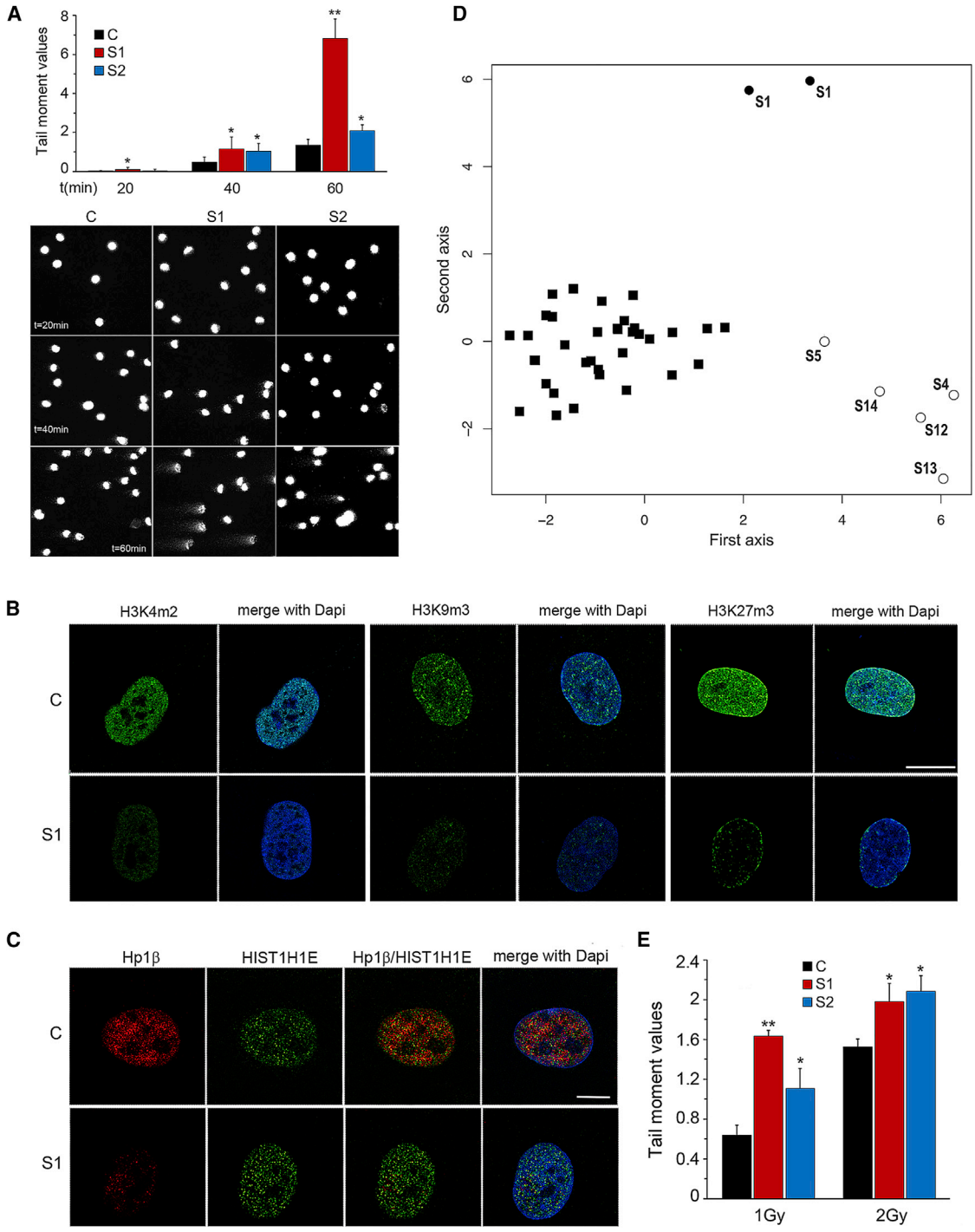

Figure 2. SCGE Assay, Immuno-Fluorescence Studies, and Methylation Profiling Analysis

(A) Increasing electrophoresis run times (20, 40, and 60 min) highlighted significant differences in relaxation of DNA supercoiling between fibroblasts from control and from affected individuals. DNA migration was quantified as Tail moment values, which are defined as the products of the tail length and the fraction of total DNA in the tail (upper panel). Nucleoids of cells from subjects S1 and S2 showed a significantly higher Tail moment value (*$p < 0.05$, **$p < 0.01$; two-tailed Student's t test). For each experimental point, at least 75 cells were analyzed. Values are mean ± SEM of three independent experiments. Representative images of nucleoids from fibroblasts from control and affected individuals at each run time are shown (lower panel).

(B) Confocal laser scanning microscopy (CLSM) observations document overall decreased amounts of H3K4me2, H3K9me3, and H3K27me3 staining (green) in S1 cells compared to control cells. Nuclei were stained with DAPI. Images are representative of >200 analyzed cells. Scale bars represent to 8 μm.

(C) Fibroblasts from subject S1 show a decreased amount of HP1β compared to control cells (WT). Cells were stained with antibodies against HP1β (red) and HIST1H1E (H1.4) (green); DNA are DAPI-stained (blue). Scale bars represent 7 μm.

(legend continued on next page)

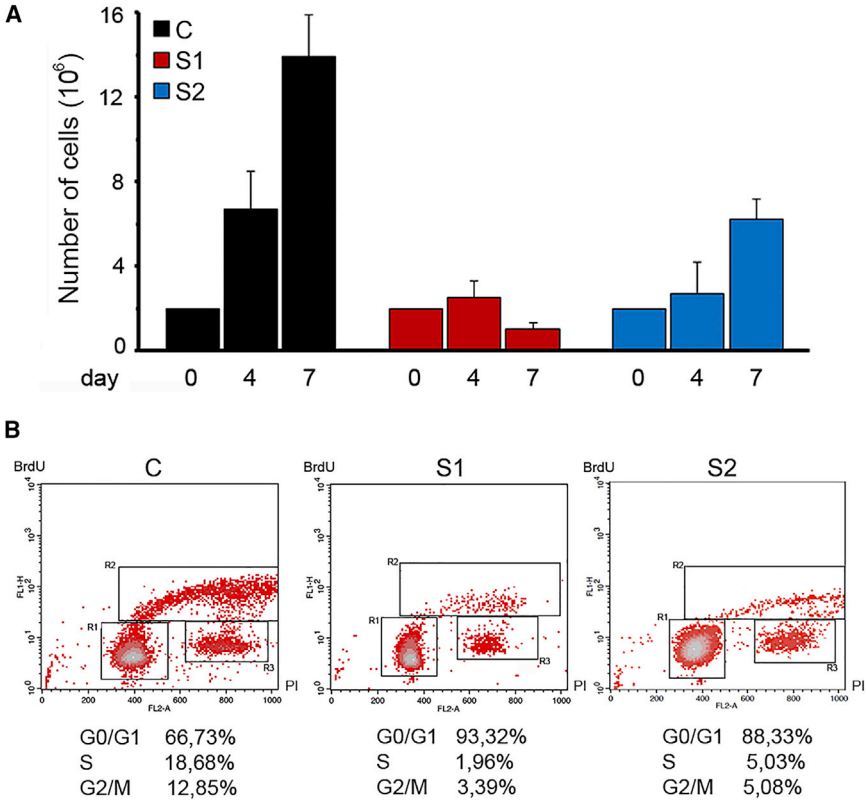

Figure 3. Proliferation Assay and Cell-Cycle Progression

(A) Cells were seeded at 200,000 cells/well in a six-well plate and incubated a 37°C. Cell numbers (mean of three replicates ± SD) were counted by trypan blue exclusion assay after four and seven days. A significantly decreased proliferation rate was observed in the fibroblast lines from the two unrelated affected individuals (S1 and S2). Cells from subject S1 show a permanent cell growth arrest.

(B) Cell cycle phases of S1/S2's (right) and control (left) fibroblasts as measured by BrdU incorporation and propidium iodide (PI) flow cytometry analysis. The upper box identifies cells incorporating BrdU (S phase), the lower left box identifies G0/G1 cells and the lower right box represents G2/M cells. One of three independent experiments is reported with the percentage of cells in each cell cycle phase.

to 1500 bp from TSS) (Table S4). Kyoto Encyclopedia of Genes and Genomes (KEGG) and Gene Ontology (GO) cellular component enrichment analyses revealed a significant enrichment of genes linked to pathways mainly related to neurological, immunological, and cell adhesion/membrane function; these represent cellular processes relevant to the clinical phenotype of affected individuals (Table S5). A separate clustering of affected pediatric individuals from controls was also observed through the use of a recently defined episignature set, which successfully profiled 14 developmental disorders (data not shown);[43] this further supports the occurrence of a specific methylation profile in people with *HIST1H1E* frameshift mutations. These findings are in line with those of previous studies performed in cells with defective histone H1 function, which showed a minor impact on global DNA methylation compared to controls. Rather, in these cells, changes involved specific CpGs within regulatory domains of regulated genes,[44] indicating that chromatin rearrangement in these cells does not globally impact the methylation status of DNA but instead affects specific subsets of genes and cellular processes.

HIST1H1E Mutations Cause Accelerated Cellular Senescence

On the basis of the occurrence of phenotypic features suggestive of premature aging and the fact that a more relaxed compaction of chromatin has been functionally linked to replicative senescence,[45] a feature occurring in progeroid syndromes,[46] we hypothesized that the aberrant function of the HIST1H1E mutants might promote accelerated senescence. To test this hypothesis, we evaluated proliferative competence and morphological and biochemical markers of cellular senescence. Trypan blue exclusion assay documented a variable but consistently reduced proliferation rate in cells from affected individuals (Figure 3A). Of note, a complete proliferative arrest was observed in S1 fibroblasts at relatively early passages. Consistent with this finding, flow-cytometry analysis documented a block in cell-cycle transition from G0/G1 to S phase (Figure 3B). Compared to control fibroblasts, those derived from affected individuals were larger and had a flattened and irregular shape. This was apparent at early passages and became more pronounced with passage of cultured cells (Figure S3). Additionally, compared to age- and passage-matched control cells, fibroblasts endogenously carrying the *HIST1H1E* mutant allele were characterized by a significantly augmented SA-β-gal activity (Figure 4A), which is an established marker of cellular senescence.[46] Furthermore, enhanced

(D) Multidimensional scaling plot of genome-wide methylation analysis using the top 1,000 most variable probes among samples. The plot shows the distinct methylation profiles of pediatric (open circles) and adult (S1, duplicate) (filled circles) affected individuals, compared to healthy controls (filled squares).

(E) DNA damage was induced by 1 or 2 Gy γ-ray irradiation. Tail moment values indicate the amount of radiation-induced DNA damage measured by SCGE assay immediately after treatment. S1 and S2 fibroblasts showed a higher sensitivity to γ-ray irradiation (*$p < 0.02$, **$p < 0.001$; two-tailed Student's t test). For each experimental point, at least 75 cells were analyzed. Values are means ± SEM of three independent experiments.

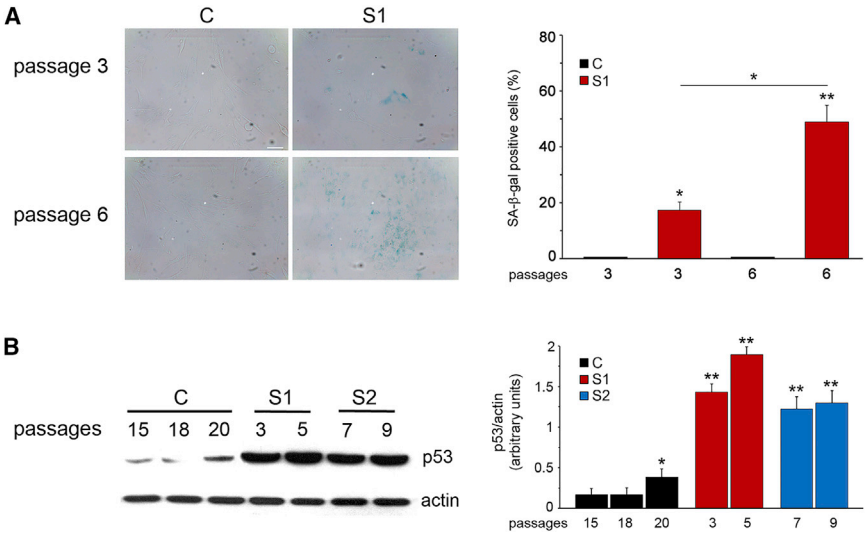

Figure 4. Defective HISTH1E Function Results in Altered SA-β-gal Activity and p53 Expression Level

(A) Representative images (left) and quantification (right) of SA-β-gal activity evaluated on S1 and control (C) fibroblasts at different culture passages. The significance was measured by one-way Anova with Tukey's multiple comparison test (*$p < 0.01$, **$p < 0.0001$).

(B) Compared to control cell lysates, fibroblast lysates from individuals S1 and S2 showed enhanced TP53 protein levels at earlier passages. Representative blots (left) and mean ± SD densitometry values (right) of three independent experiments are shown (*$p < 0.05$, **$p < 0.002$; two-tailed Student's t test).

levels of TP53, whose amount increases during replicative senescence,[47] were observed at early passages (Figure 4B). These data demonstrate a direct link between aberrant HIST1H1E function and replicative senescence.

In premature-aging disorders, replicative senescence can be caused by multiple events, including DNA double-strand breaks (DSBs), telomere dysfunction and/or accelerated shortening, and lamin defects.[48–50] To evaluate the telomere status, we first performed Q-FISH analysis, which showed no difference in telomere length between control cells and fibroblasts from affected individuals (Figure S4A). Immunofluorescence analysis designed to identify γH2AX foci, markers of DSBs,[51] showed an increased number of positive cells and foci *per* cell among those carrying mutant HIST1H1E compared to control cells (Figure S4B), indicating increased spontaneous DNA damage. ImmunoFISH analysis also documented a higher frequency of co-localization between γH2AX foci and telomeres in cells from affected individuals than in control cells (Figure S4C), highlighting the presence of dysfunctional telomeres in these cells. Fibroblasts carrying the mutated *HIST1H1E* allele also showed a higher sensitivity to low doses of γ-ray irradiation (Figure 2E), documenting augmented susceptibility to DNA damage. These findings suggest that the proliferative arrest and senescent phenotype of cells expressing the mutant *HIST1H1E* allele might result, at least in part, from ineffective DNA repair and persistent activation of DNA damage response (DDR) signaling.[52,53] To explore this possibility, the fraction of residual DNA damage was evaluated by SCGE assay post-γ-ray irradiation. Kinetics data documented defective and/or delayed DNA repair of single-strand breaks and DSBs in mutant fibroblasts compared to control cells (Figure S5).

Cells carrying *LMNA* (MIM: 150330) gene mutations that drive cellular senescence exhibit characteristic morphological nuclear abnormalities due to altered mechanical properties of the lamina,[54] a network of structural filaments that interact with chromatin to participate in chromatin remodeling and organization as well as DNA replication and transcription.[55–58] Thus, we explored possible changes in nuclear morphology and architecture. Immunofluorescence analysis showed aberrant lamin A/C morphology in cells that were taken from affected individuals and induced to divide after thymidine/nocodazole treatment (Figure 5A). Aberrant morphology ranged from abnormal nuclear shapes to nuclear blebbing. Of note, an increased number of aberrantly shaped nuclei in fibroblasts carrying the *HIST1H1E* frameshift was observed at early passages in cells from affected individuals compared to control cells, and this difference became more pronounced as passages increased ($p < 0.0000001$; two-tails Fisher's exact test) (Figure 5B). This feature is reminiscent of changes in nuclear shape in progeroid syndromes and confirms the senescent phenotype associated with aberrant HIST1H1E function.

HIST1H1E Mutations Trigger Nucleolar Instability

Heterochromatin plays a role in maintaining nucleolar stability and controlling rRNA synthesis,[59] and decreased heterochromatin levels have been associated with nucleolar instability and upregulated transcription of rRNA genes that, in turn, has been suggested to enhance protein synthesis and contribute to overgrowth and accelerated aging.[60,61] Besides functioning in ribosome biogenesis, the nucleolus is involved in cell-cycle control,[62] and linker histones have been reported to interact with multiple nucleolar proteins that are implicated in various nucleolar functions.[63] On the basis of these considerations, we explored whether *HIST1H1E* mutations trigger nucleolar instability. As shown, S1 fibroblasts displayed fragmentation of the nucleolus, as revealed by loss of the nucleolar marker nucleolin (Figure 6A), and these fibroblasts also showed increased 28S rRNA levels and an increased amount of 18S (Figure 6B); these results

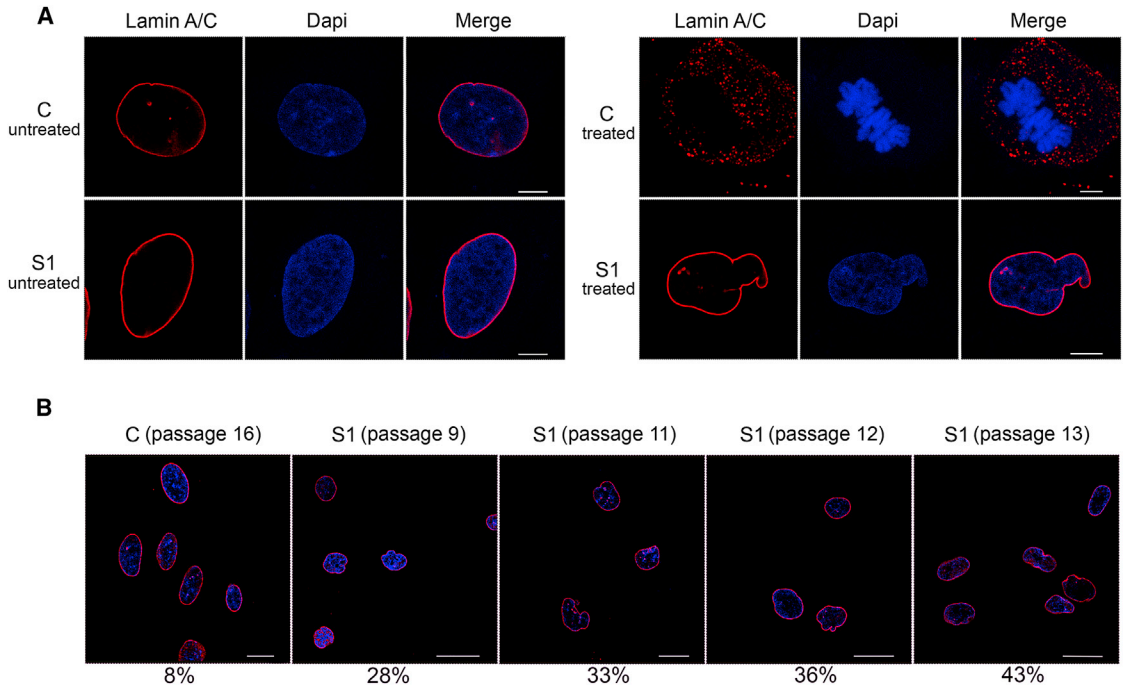

Figure 5. Defective HISTH1E Function Results in Aberrant Nuclear Morphology That Is Exacerbated over Cell-Culture Passages
(A) CLSM analysis was performed in steady-state (left) and synchronized (right) skin fibroblasts induced to divide after being treated with thymidine/nocodazole and recovered with fresh medium. The panels show an aberrant nuclear morphology in cells from subject S1. Whereas control cells proceed through mitosis (representative metaphases are shown), S1 fibroblasts fail to progress. Experiments were carried out at early passages (passage 3). Cells were stained with an antibody against lamin A/C (red) and DAPI (blue). Images are representative of >200 analyzed cells. Scale bars represent 7 μm.
(B) CLSM analysis was performed on S1 and control fibroblasts seeded at different culture passages. The panels show an aberrant nuclear morphology at early passages in subject S1's cells compared to control cells, which were seeded at late passages (passage 16). Percentages refer to the number of cells with aberrant nuclear morphology. Cells were stained as above. Images are representative of >200 analyzed cells. Scale bars represent 27 μm.

further document the pleiotropic effect of *HIST1H1E* mutations. Notably, these findings suggest that besides affecting nucleolar function, dysregulated rRNA synthesis driven by *HIST1H1E* frameshift mutations might represent the molecular event causally linked to macrosomia, a recurring feature among young children with this class of mutations.[19,20] This hypothesis is in line with other observations correlating tissue plasticity to ribosomal biogenesis, as documented for the skeletal muscle mass modulated by seasonal acclimatization in *Cyprinus carpio*.[64]

Aneuploidy Is a Major Feature of Cells Bearing *HIST1H1E* Frameshift

Finally, because maximal chromatin compaction is required for proper chromosomal segregation and aneuploidy is a marker of the chromosomal instability which characterizes the senescent phenotype, we expected the occurrence of aneuploidy in cells expressing the disease-causing HIST1H1E mutants. Indeed, direct count of chromosomes in metaphases revealed a remarkably high proportion of aneuploidy in early-passage fibroblasts from S1 (41.2% of analyzed cells), which was significantly higher even when compared to late-passage control fibroblasts (18.9% of cells) ($p < 0.01$, χ^2 test).

Discussion

Here we show that a specific class of dominantly acting frameshift mutations affecting the C-terminal tail of HIST1H1E disrupts chromatin structure and nuclear lamina organization and drives cellular replicative senescence. By assessing the clinical records of a relatively large cohort of individuals carrying these mutations, we also show that this endophenotype is mirrored by features suggestive of accelerated aging.

HIST1H1E is one of the members of the linker histone family, whose members function as structural components of chromatin to control the extent of DNA compaction and contribute to the regulation of gene expression and DNA replication, recombination, and repair.[4,6,8,44] Linker histones are encoded by multiple genes in the mammalian genomes; such genes include paralogs characterized by a diverse expression pattern during development and having either a ubiquitous distribution or an expression restricted to specific cell types.[9,65] Among these, *HIST1H1E* has been reported to be expressed ubiquitously at a high level,[65] and similarly to the other replication-dependent linker histones, HIST1H1E is synthetized during the S phase to assemble chromatin with newly replicated DNA.[66] As with the other linker histones, the protein is

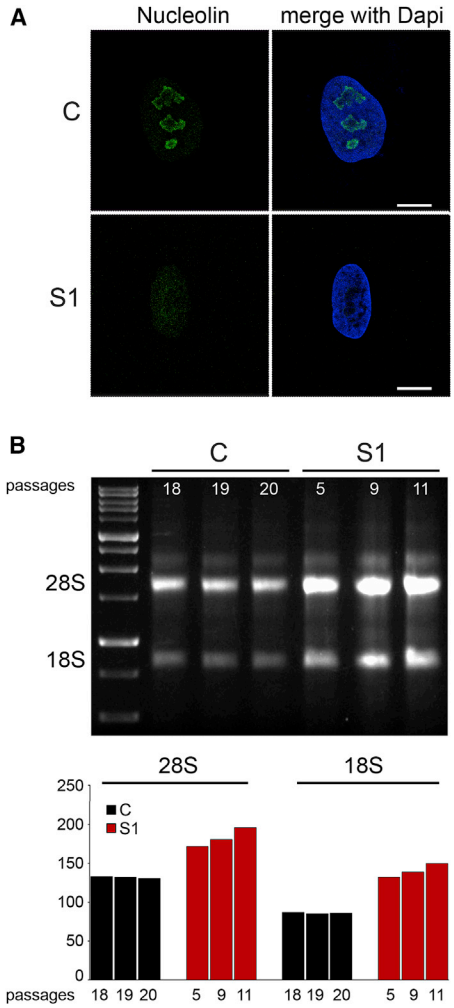

Figure 6. Defective HIST1H1E Function Results in Nucleolar Fragmentation and Increased 18S and 28S rRNA Levels
(A) CLSM observations were performed on S1 and control (C) fibroblasts. Panels show a significant decrease in C3 clone antibody staining in S1 fibroblasts, revealing nucleolar fragmentation. Nuclei were stained with DAPI. Images are representative of >200 analyzed cells. Scale bars represent 9 μm.
(B) Total RNA was extracted from the same amount of S1 and C cells at different cellular passages. Three μl of total RNA was loaded for size separation on 1% agarose gel and stained with ethidium bromide. Increased amounts (compared to those in control cells) of both 28S and 18S rRNA codifying for ribosomal subunits are evident in fibroblasts from subject S1.

relatively depleted from active promoters and other regulatory regions controlling transcription and enriched in portions of the genome carrying repressive histone marks.[6] Notably, previous studies provided evidence that inactivation of any of this class of histones does not significantly perturb murine development, which is compromised only when a concomitant inactivation of multiple subtypes occurs, resulting in an extensive reduction of these proteins.[10,11] Consistent with this functional redundancy, our data do not support haploinsufficiency as the molecular mechanism implicated in pathogenesis (see below) but point to a specific, dominantly acting effect causing a profound perturbation of multiple cellular processes directly and indirectly controlled by chromatin remodeling. Such pleiotropic effects involve genome instability, epigenetic modifications, inefficient DNA repair ability, improper chromosome compaction and segregation, and nucleolar fragmentation, converging toward cellular senescence and replicative impasse.

Similar to what is observed in progeroid disorders (e.g., Hutchinson-Gilford progeria [MIM: 176670], Werner syndrome [MIM: 277700], and lipodystrophy syndromes), the cellular processes affected in the disorder associated with aberrant HIST1H1E function, link cellular senescence to premature aging. The clinical profile of the affected individuals with *HIST1H1E* mutations, however, differs from those of individuals with progeroid disorders, and this profile is quite peculiar. The main features are a distinctive facies characterized by bitemporal narrowing, macrocephaly, prominent forehead, high anterior hairline, sparse frontotemporal hair, hypertelorism, downslanted palpebral fissures, a broad nasal tip, and low-set and posteriorly rotated ears. DD/ID invariantly occurs, whereas overgrowth, which had been originally reported as a key feature of the disorder, was not observed in any of the subjects included in this work at last assessment; this suggests that enhanced growth might represent a feature characterizing infancy. Although the facial gestalt can help in recognition of the disorder, we noted that no pathognomonic features can be used for a definitive clinical diagnosis. In early childhood, a tentative differential diagnosis should include Pallister-Killian syndrome and mild phenotypes within the spectrum of Weaver syndrome, Werner syndrome, and other progeroid disorders.

Besides documenting the multiple events contributing to cellular senescence, the present findings provide a mechanistic model for the multifaceted impact of this class of *HIST1H1E* mutations. Our data further document the specific and narrow spectrum of disease causative mutations affecting this gene. The long, lysine-rich C-terminal tail of HIST1H1E encompasses multiple regulatory residues that are substrates for cyclin-dependent kinases, and the extent of phosphorylation controls the proper compaction required for chromosome segregation, as well as local chromatin decondensation needed to promote DNA transcription, replication, and repair. The phosphorylation of this region during the cell cycle has been theorized to contribute to the control of the chromatin state by a twofold process.[3,4,12,67] Partial phosphorylation is attained during interphase (G0–S phase), allowing dynamical chromatin relaxation and access to DNA.[68–70] On the other hand, a maximal phosphorylation is attained during mitosis (M phase), which is considered to be required for chromatin condensation and segregation of chromosomes into daughter cells during cell division.[71–75] In this context, the functionally equivalent disease-causing frameshift events are the only mutations that are predicted to not significantly affect the capability of the mutant protein to retain efficient chromatin binding with concomitant loss of the regulatory sites required for

modulation of higher-order chromatin architecture. Consistent with this model, the *HIST1H1E* truncating variants reported in gnomAD affect regions of the protein that do not overlap the mutational hotspot here defined but are much more proximal to the N terminus or to the C terminus (Figure S6). The former are predicted to result in truncated proteins with defective binding to chromatin and/or expected to undergo accelerated degradation, whereas the latter retain the regulatory serine/threonine residues and are not expected to have a dominant negative effect. The complexity by which the C-terminal tail controls HIST1H1E function, the high stability of these mutants, and their ability to bind to chromatin strongly support the possibility of a dominant negative effect of these mutants. However, neomorphism or gain-of-function as alternative mechanism(s) of disease cannot be ruled out *a priori*, and experimentally testing the different models will require dedicated studies.

Taken together, the present findings provide evidence that dominantly acting functional dysregulation of a linker histone causes a complex cellular phenotype characterized by replicative senescence and results in a neurodevelopmental disorder characterized by accelerated aging.

Accession Numbers

All mutations identified in this work have been submitted to ClinVar (submission IDs: SCV000925231 to SCV000925238).

Supplemental Data

Supplemental Data can be found online at https://doi.org/10.1016/j.ajhg.2019.07.007.

Acknowledgments

We thank the patients and their families for their participation in this study, and Serenella Venanzi (Istituto Superiore di Sanità, Rome) for technical support. This project was supported, in part, by Fondazione Bambino Gesù (Vite Coraggiose to M.T.), the Italian Ministry of Health (Ricerca Corrente 2017 and 2018 to A.C. and M.T.), Associazione Italiana per la Ricerca sul Cancro (AIRC) (IG21390 to G.M. and IG21614 to M.T.) and Ministero dell'Istruzione, dell'Università e della Ricerca (MIUR) Dipartimenti di Eccellenza (miur)(Project D15D18000410001) to the Department of Medical Sciences, University of Turin, Italy. M.T. acknowledges Consorsio Interuniversitario per il Calcolo Automatico (CINECA) for the computational resources. The Broad Center for Mendelian Genomics (UM1 HG008900) is funded by the National Human Genome Research Institute with supplemental funding provided by the National Heart, Lung, and Blood Institute under the Trans-Omics for Precision Medicine (TOPMed) program and the National Eye Institute. M.H.W. is supported by National Institutes of Health (NIH) grant T32GM007748. R.F.K. and A.V.D. are supported by grants from the European Research Area Network (ERA-NET) NEURON through the Research Foundation—Flanders - (FWO). K.Õ., S.P., and K.R. are supported by Estonian Research Council grants PRG471 and PUTJD827.

Declaration of Interests

A.Be. and R.P. declare no additional conflicts of interest beyond their employment affiliation. All of the other authors declare no competing interests.

Received: April 6, 2019
Accepted: July 10, 2019
Published: August 22, 2019

Web Resources

Combined Annotation Dependent Depletion (CADD), https://cadd.gs.washington.edu/
Database for nonsynonymous SNPs' functional predictions (dbNSFP), https://sites.google.com/site/jpopgen/dbNSFP
ExAC database, http://exac.broadinstitute.org/
Gene, https://www.ncbi.nlm.nih.gov/gene/
Gene SeT AnaLysis, http://www.webgestalt.org/option.php
GnomAD, https://gnomad.broadinstitute.org/
Online Mendelian Inheritance in Man (OMIM), https://www.omim.org/

References

1. Wolffe, A. (1998). Chromatin: Structure and function (London: Academic Press).
2. Luger, K., Mäder, A.W., Richmond, R.K., Sargent, D.F., and Richmond, T.J. (1997). Crystal structure of the nucleosome core particle at 2.8 A resolution. Nature *389*, 251–260.
3. Harshman, S.W., Young, N.L., Parthun, M.R., and Freitas, M.A. (2013). H1 histones: current perspectives and challenges. Nucleic Acids Res. *41*, 9593–9609.
4. Hergeth, S.P., and Schneider, R. (2015). The H1 linker histones: multifunctional proteins beyond the nucleosomal core particle. EMBO Rep. *16*, 1439–1453.
5. Crane-Robinson, C. (2016). Linker histones: History and current perspectives. Biochim. Biophys. Acta *1859*, 431–435.
6. Izzo, A., Kamieniarz-Gdula, K., Ramírez, F., Noureen, N., Kind, J., Manke, T., van Steensel, B., and Schneider, R. (2013). The genomic landscape of the somatic linker histone subtypes H1.1 to H1.5 in human cells. Cell Rep. *3*, 2142–2154.
7. Geeven, G., Zhu, Y., Kim, B.J., Bartholdy, B.A., Yang, S.M., Macfarlan, T.S., Gifford, W.D., Pfaff, S.L., Verstegen, M.J., Pinto, H., et al. (2015). Local compartment changes and regulatory landscape alterations in histone H1-depleted cells. Genome Biol. *16*, 289.
8. Bayona-Feliu, A., Casas-Lamesa, A., Reina, O., Bernués, J., and Azorín, F. (2017). Linker histone H1 prevents R-loop accumulation and genome instability in heterochromatin. Nat. Commun. *8*, 283.
9. Pan, C., and Fan, Y. (2016). Role of H1 linker histones in mammalian development and stem cell differentiation. Biochim. Biophys. Acta *1859*, 496–509.
10. Sirotkin, A.M., Edelmann, W., Cheng, G., Klein-Szanto, A., Kucherlapati, R., and Skoultchi, A.I. (1995). Mice develop normally without the H1(0) linker histone. Proc. Natl. Acad. Sci. USA *92*, 6434–6438.
11. Fan, Y., Sirotkin, A., Russell, R.G., Ayala, J., and Skoultchi, A.I. (2001). Individual somatic H1 subtypes are dispensable for mouse development even in mice lacking the H1(0) replacement subtype. Mol. Cell. Biol. *21*, 7933–7943.

12. Liao, R., and Mizzen, C.A. (2016). Interphase H1 phosphorylation: Regulation and functions in chromatin. Biochim. Biophys. Acta *1859*, 476–485.
13. Kurotaki, N., Imaizumi, K., Harada, N., Masuno, M., Kondoh, T., Nagai, T., Ohashi, H., Naritomi, K., Tsukahara, M., Makita, Y., et al. (2002). Haploinsufficiency of NSD1 causes Sotos syndrome. Nat. Genet. *30*, 365–366.
14. Ng, S.B., Bigham, A.W., Buckingham, K.J., Hannibal, M.C., McMillin, M.J., Gildersleeve, H.I., Beck, A.E., Tabor, H.K., Cooper, G.M., Mefford, H.C., et al. (2010). Exome sequencing identifies MLL2 mutations as a cause of Kabuki syndrome. Nat. Genet. *42*, 790–793.
15. Qi, H.H., Sarkissian, M., Hu, G.Q., Wang, Z., Bhattacharjee, A., Gordon, D.B., Gonzales, M., Lan, F., Ongusaha, P.P., Huarte, M., et al. (2010). Histone H4K20/H3K9 demethylase PHF8 regulates zebrafish brain and craniofacial development. Nature *466*, 503–507.
16. Yuen, B.T., and Knoepfler, P.S. (2013). Histone H3.3 mutations: A variant path to cancer. Cancer Cell *24*, 567–574.
17. Maze, I., Noh, K.M., Soshnev, A.A., and Allis, C.D. (2014). Every amino acid matters: essential contributions of histone variants to mammalian development and disease. Nat. Rev. Genet. *15*, 259–271.
18. Tessadori, F., Giltay, J.C., Hurst, J.A., Massink, M.P., Duran, K., Vos, H.R., van Es, R.M., Deciphering Developmental Disorders Study, Scott, R.H., van Gassen, K.L.I., Bakkers, J., and van Haaften, G. (2017). Germline mutations affecting the histone H4 core cause a developmental syndrome by altering DNA damage response and cell cycle control. Nat. Genet. *49*, 1642–1646.
19. Tatton-Brown, K., Loveday, C., Yost, S., Clarke, M., Ramsay, E., Zachariou, A., Elliott, A., Wylie, H., Ardissone, A., Rittinger, O., et al. (2017). Mutations in epigenetic regulation genes are a major cause of overgrowth with intellectual disability. Am. J. Hum. Genet. *100*, 725–736.
20. Takenouchi, T., Uehara, T., Kosaki, K., and Mizuno, S. (2018). Growth pattern of Rahman syndrome. Am. J. Med. Genet. A. *176*, 712–714.
21. Flex, E., Niceta, M., Cecchetti, S., Thiffault, I., Au, M.G., Capuano, A., Piermarini, E., Ivanova, A.A., Francis, J.W., Chillemi, G., et al. (2016). Biallelic mutations in TBCD, encoding the tubulin folding cofactor d, perturb microtubule dynamics and cause early-onset encephalopathy. Am. J. Hum. Genet. *99*, 962–973.
22. Bauer, C.K., Calligari, P., Radio, F.C., Caputo, V., Dentici, M.L., Falah, N., High, F., Pantaleoni, F., Barresi, S., Ciolfi, A., et al. (2018). Mutations in KCNK4 that affect gating cause a recognizable neurodevelopmental syndrome. Am. J. Hum. Genet. *103*, 621–630.
23. Dorboz, I., Aiello, C., Simons, C., Stone, R.T., Niceta, M., Elmaleh, M., Abuawad, M., Doummar, D., Bruselles, A., Wolf, N.I., et al. (2017). Biallelic mutations in the homeodomain of NKX6-2 underlie a severe hypomyelinating leukodystrophy. Brain *140*, 2550–2556.
24. Yang, Y., Muzny, D.M., Xia, F., Niu, Z., Person, R., Ding, Y., Ward, P., Braxton, A., Wang, M., Buhay, C., et al. (2014). Molecular findings among patients referred for clinical whole-exome sequencing. JAMA *312*, 1870–1879.
25. Vandeweyer, G., Van Laer, L., Loeys, B., Van den Bulcke, T., and Kooy, R.F. (2014). VariantDB: A flexible annotation and filtering portal for next generation sequencing data. Genome Med. *6*, 74.
26. Lek, M., Karczewski, K.J., Minikel, E.V., Samocha, K.E., Banks, E., Fennell, T., O'Donnell-Luria, A.H., Ware, J.S., Hill, A.J., Cummings, B.B., et al. (2016). Analysis of protein-coding genetic variation in 60,706 humans. Nature *536*, 285–291.
27. Retterer, K., Juusola, J., Cho, M.T., Vitazka, P., Millan, F., Gibellini, F., Vertino-Bell, A., Smaoui, N., Neidich, J., Monaghan, K.G., et al. (2016). Clinical application of whole-exome sequencing across clinical indications. Genet. Med. *18*, 696–704.
28. Andreoli, C., Leopardi, P., and Crebelli, R. (1997). Detection of DNA damage in human lymphocytes by alkaline single cell gel electrophoresis after exposure to benzene or benzene metabolites. Mutat. Res. *377*, 95–104.
29. Catanzaro, G., Besharat, Z.M., Miele, E., Chiacchiarini, M., Po, A., Carai, A., Marras, C.E., Antonelli, M., Badiali, M., Raso, A., et al. (2018). The miR-139-5p regulates proliferation of supratentorial paediatric low-grade gliomas by targeting the PI3K/AKT/mTORC1 signalling. Neuropathol. Appl. Neurobiol. *44*, 687–706.
30. Zhou, C., Cunningham, L., Marcus, A.I., Li, Y., and Kahn, R.A. (2006). Arl2 and Arl3 regulate different microtubule-dependent processes. Mol. Biol. Cell *17*, 2476–2487.
31. Cordeddu, V., Redeker, B., Stellacci, E., Jongejan, A., Fragale, A., Bradley, T.E., Anselmi, M., Ciolfi, A., Cecchetti, S., Muto, V., et al. (2014). Mutations in ZBTB20 cause Primrose syndrome. Nat. Genet. *46*, 815–817.
32. Berardinelli, F., Antoccia, A., Buonsante, R., Gerardi, S., Cherubini, R., De Nadal, V., Tanzarella, C., and Sgura, A. (2013). The role of telomere length modulation in delayed chromosome instability induced by ionizing radiation in human primary fibroblasts. Environ. Mol. Mutagen. *54*, 172–179.
33. Perner, S., Brüderlein, S., Hasel, C., Waibel, I., Holdenried, A., Ciloglu, N., Chopurian, H., Nielsen, K.V., Plesch, A., Högel, J., and Möller, P. (2003). Quantifying telomere lengths of human individual chromosome arms by centromere-calibrated fluorescence in situ hybridization and digital imaging. Am. J. Pathol. *163*, 1751–1756.
34. Morris, T.J., Butcher, L.M., Feber, A., Teschendorff, A.E., Chakravarthy, A.R., Wojdacz, T.K., and Beck, S. (2014). Champ: 450k chip analysis methylation pipeline. Bioinformatics *30*, 428–430.
35. Guarrera, S., Fiorito, G., Onland-Moret, N.C., Russo, A., Agnoli, C., Allione, A., Di Gaetano, C., Mattiello, A., Ricceri, F., Chiodini, P., et al. (2015). Gene-specific DNA methylation profiles and LINE-1 hypomethylation are associated with myocardial infarction risk. Clin. Epigenetics *7*, 133.
36. Wang, J., Vasaikar, S., Shi, Z., Greer, M., and Zhang, B. (2017). WebGestalt 2017: A more comprehensive, powerful, flexible and interactive gene set enrichment analysis toolkit. Nucleic Acids Res. *45*, 130–137.
37. Sobreira, N., Schiettecatte, F., Valle, D., and Hamosh, A. (2015). GeneMatcher: A matching tool for connecting investigators with an interest in the same gene. Hum. Mutat. *36*, 928–930.
38. Duffney, L.J., Valdez, P., Tremblay, M.W., Cao, X., Montgomery, S., McConkie-Rosell, A., and Jiang, Y.H. (2018). Epigenetics and autism spectrum disorder: A report of an autism case with mutation in H1 linker histone HIST1H1E and literature review. Am. J. Med. Genet. B. Neuropsychiatr. Genet. *177*, 426–433.
39. Helsmoortel, C., Vandeweyer, G., Ordoukhanian, P., Van Nieuwerburgh, F., Van der Aa, N., and Kooy, R.F. (2015).

Challenges and opportunities in the investigation of unexplained intellectual disability using family-based whole-exome sequencing. Clin. Genet. *88*, 140–148.
40. Kouzarides, T. (2007). Chromatin modifications and their function. Cell *128*, 693–705.
41. Daujat, S., Zeissler, U., Waldmann, T., Happel, N., and Schneider, R. (2005). HP1 binds specifically to Lys26-methylated histone H1.4, whereas simultaneous Ser27 phosphorylation blocks HP1 binding. J. Biol. Chem. *280*, 38090–38095.
42. Allis, C.D., and Jenuwein, T. (2016). The molecular hallmarks of epigenetic control. Nat. Rev. Genet. *17*, 487–500.
43. Aref-Eshghi, E., Bend, E.G., Colaiacovo, S., Caudle, M., Chakrabarti, R., Napier, M., Brick, L., Brady, L., Carere, D.A., Levy, M.A., et al. (2019). Diagnostic utility of genome-wide DNA methylation testing in genetically unsolved individuals with suspected hereditary conditions. Am. J. Hum. Genet. *104*, 685–700.
44. Fan, Y., Nikitina, T., Zhao, J., Fleury, T.J., Bhattacharyya, R., Bouhassira, E.E., Stein, A., Woodcock, C.L., and Skoultchi, A.I. (2005). Histone H1 depletion in mammals alters global chromatin structure but causes specific changes in gene regulation. Cell *123*, 1199–1212.
45. Criscione, S.W., Teo, Y.V., and Neretti, N. (2016). The chromatin landscape of cellular senescence. Trends Genet. *32*, 751–761.
46. López-Otín, C., Blasco, M.A., Partridge, L., Serrano, M., and Kroemer, G. (2013). The hallmarks of aging. Cell *153*, 1194–1217.
47. Kulju, K.S., and Lehman, J.M. (1995). Increased p53 protein associated with aging in human diploid fibroblasts. Exp. Cell Res. *217*, 336–345.
48. Cau, P., Navarro, C., Harhouri, K., Roll, P., Sigaudy, S., Kaspi, E., Perrin, S., De Sandre-Giovannoli, A., and Lévy, N. (2014). Nuclear matrix, nuclear envelope and premature aging syndromes in a translational research perspective. Semin. Cell Dev. Biol. *29*, 125–147.
49. Rossiello, F., Herbig, U., Longhese, M.P., Fumagalli, M., and d'Adda di Fagagna, F. (2014). Irreparable telomeric DNA damage and persistent DDR signalling as a shared causative mechanism of cellular senescence and ageing. Curr. Opin. Genet. Dev. *26*, 89–95.
50. Lidzbarsky, G., Gutman, D., Shekhidem, H.A., Sharvit, L., and Atzmon, G. (2018). Genomic instabilities, cellular senescence, and aging: In vitro, in vivo and aging-like human syndromes. Front. Med. *5*, 104.
51. Sedelnikova, O.A., and Bonner, W.M. (2006). GammaH2AX in cancer cells: A potential biomarker for cancer diagnostics, prediction and recurrence. Cell Cycle *5*, 2909–2913.
52. Downey, M., and Durocher, D. (2006). GammaH2AX as a checkpoint maintenance signal. Cell Cycle *5*, 1376–1381.
53. Fillingham, J., Keogh, M.C., and Krogan, N.J. (2006). GammaH2AX and its role in DNA double-strand break repair. Biochem. Cell Biol. *84*, 568–577.
54. Dahl, K.N., Scaffidi, P., Islam, M.F., Yodh, A.G., Wilson, K.L., and Misteli, T. (2006). Distinct structural and mechanical properties of the nuclear lamina in Hutchinson-Gilford progeria syndrome. Proc. Natl. Acad. Sci. USA *103*, 10271–10276.
55. Broers, J.L., Ramaekers, F.C., Bonne, G., Yaou, R.B., and Hutchison, C.J. (2006). Nuclear lamins: Laminopathies and their role in premature ageing. Physiol. Rev. *86*, 967–1008.
56. Gruenbaum, Y., and Foisner, R. (2015). Lamins: nuclear intermediate filament proteins with fundamental functions in nuclear mechanics and genome regulation. Annu. Rev. Biochem. *84*, 131–164.
57. Shumaker, D.K., Dechat, T., Kohlmaier, A., Adam, S.A., Bozovsky, M.R., Erdos, M.R., Eriksson, M., Goldman, A.E., Khuon, S., Collins, F.S., et al. (2006). Mutant nuclear lamin A leads to progressive alterations of epigenetic control in premature aging. Proc. Natl. Acad. Sci. USA *103*, 8703–8708.
58. Gonzalez-Suarez, I., and Gonzalo, S. (2010). Nurturing the genome: A-type lamins preserve genomic stability. Nucleus *1*, 129–135.
59. Padeken, J., and Heun, P. (2014). Nucleolus and nuclear periphery: velcro for heterochromatin. Curr. Opin. Cell Biol. *28*, 54–60.
60. Larson, K., Yan, S.J., Tsurumi, A., Liu, J., Zhou, J., Gaur, K., Guo, D., Eickbush, T.H., and Li, W.X. (2012). Heterochromatin formation promotes longevity and represses ribosomal RNA synthesis. PLoS Genet. *8*, e1002473.
61. Tsekrekou, M., Stratigi, K., and Chatzinikolaou, G. (2017). The nucleolus: In genome maintenance and repair. Int. J. Mol. Sci. *18*, pii: E1411.
62. Pederson, T. (2011). The nucleolus. Cold Spring Harb. Perspect. Biol. *3*, a000638.
63. Kalashnikova, A.A., Rogge, R.A., and Hansen, J.D. (2016). Linker histone H1 and protein-protein interactions. Biochim. Biophys. Acta *1859*, 455–461.
64. Fuentes, E.N., Zuloaga, R., Valdes, J.A., Molina, A., and Alvarez, M. (2014). Skeletal muscle plasticity induced by seasonal acclimatization involves IGF1 signaling: implications in ribosomal biogenesis and protein synthesis. Comp. Biochem. Physiol. B Biochem. Mol. Biol. *176*, 48–57.
65. Parseghian, M.H., and Hamkalo, B.A. (2001). A compendium of the histone H1 family of somatic subtypes: an elusive cast of characters and their characteristics. Biochem. Cell Biol. *79*, 289–304.
66. Happel, N., Warneboldt, J., Hänecke, K., Haller, F., and Doenecke, D. (2009). H1 subtype expression during cell proliferation and growth arrest. Cell Cycle *8*, 2226–2232.
67. Roque, A., Ponte, I., and Suau, P. (2016). Interplay between histone H1 structure and function. Biochim. Biophys. Acta *1859*, 444–454.
68. Chadee, D.N., Taylor, W.R., Hurta, R.A., Allis, C.D., Wright, J.A., and Davie, J.R. (1995). Increased phosphorylation of histone H1 in mouse fibroblasts transformed with oncogenes or constitutively active mitogen-activated protein kinase. J. Biol. Chem. *270*, 20098–20105.
69. Herrera, R.E., Chen, F., and Weinberg, R.A. (1996). Increased histone H1 phosphorylation and relaxed chromatin structure in Rb-deficient fibroblasts. Proc. Natl. Acad. Sci. USA *93*, 11510–11515.
70. Chadee, D.N., Allis, C.D., Wright, J.A., and Davie, J.R. (1997). Histone H1b phosphorylation is dependent upon ongoing transcription and replication in normal and ras-transformed mouse fibroblasts. J. Biol. Chem. *272*, 8113–8116.
71. Gurley, L.R., Walters, R.A., and Tobey, R.A. (1975). Sequential phosphorylation of histone subfractions in the Chinese hamster cell cycle. J. Biol. Chem. *250*, 3936–3944.
72. Hohmann, P., Tobey, R.A., and Gurley, L.R. (1976). Phosphorylation of distinct regions of f1 histone. Relationship to the cell cycle. J. Biol. Chem. *251*, 3685–3692.

73. Gurley, L.R., D'Anna, J.A., Barham, S.S., Deaven, L.L., and Tobey, R.A. (1978). Histone phosphorylation and chromatin structure during mitosis in Chinese hamster cells. Eur. J. Biochem. *84*, 1–15.
74. Matsumoto, Y., Yasuda, H., Mita, S., Marunouchi, T., and Yamada, M. (1980). Evidence for the involvement of H1 histone phosphorylation in chromosome condensation. Nature *284*, 181–183.
75. Ajiro, K., Borun, T.W., and Cohen, L.H. (1981). Phosphorylation states of different histone 1 subtypes and their relationship to chromatin functions during the HeLa S-3 cell cycle. Biochemistry *20*, 1445–1454.

The American Journal of Human Genetics, Volume *105*

Supplemental Data

Aberrant Function of the C-Terminal Tail of HIST1H1E Accelerates Cellular Senescence and Causes Premature Aging

Elisabetta Flex, Simone Martinelli, Anke Van Dijck, Andrea Ciolfi, Serena Cecchetti, Elisa Coluzzi, Luca Pannone, Cristina Andreoli, Francesca Clementina Radio, Simone Pizzi, Giovanna Carpentieri, Alessandro Bruselles, Giuseppina Catanzaro, Lucia Pedace, Evelina Miele, Elena Carcarino, Xiaoyan Ge, Chieko Chijiwa, M.E. Suzanne Lewis, Marije Meuwissen, Sandra Kenis, Nathalie Van der Aa, Austin Larson, Kathleen Brown, Melissa P. Wasserstein, Brian G. Skotko, Amber Begtrup, Richard Person, Maria Karayiorgou, J. Louw Roos, Koen L. Van Gassen, Marije Koopmans, Emilia K. Bijlsma, Gijs W.E. Santen, Daniela Q.C.M. Barge-Schaapveld, Claudia A.L. Ruivenkamp, Mariette J.V. Hoffer, Seema R. Lalani, Haley Streff, William J. Craigen, Brett H. Graham, Annette P.M. van den Elzen, Daan J. Kamphuis, Katrin Õunap, Karit Reinson, Sander Pajusalu, Monica H. Wojcik, Clara Viberti, Cornelia Di Gaetano, Enrico Bertini, Simona Petrucci, Alessandro De Luca, Rossella Rota, Elisabetta Ferretti, Giuseppe Matullo, Bruno Dallapiccola, Antonella Sgura, Magdalena Walkiewicz, R. Frank Kooy, and Marco Tartaglia

SUPPLEMENTAL FIGURES

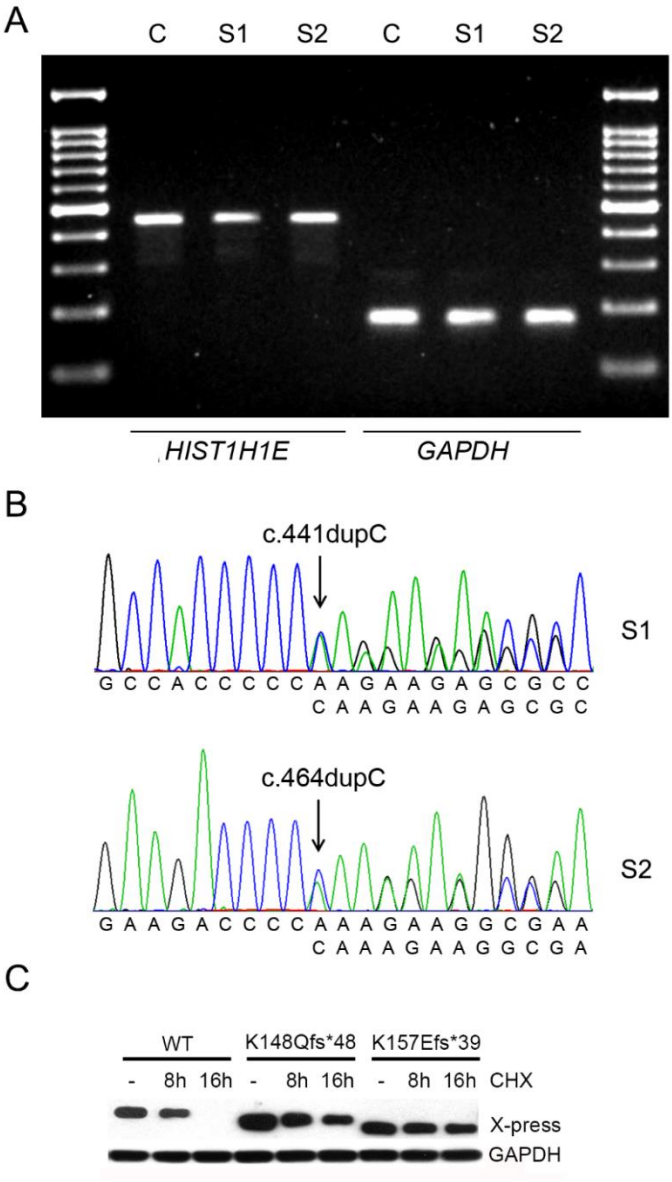

Figure S1. Disease-causing *HIST1H1E* frameshift mutations do not affect RNA and protein stability. (**A**) RT-PCR products obtained from total RNA from fibroblasts of affected subjects S1 and S2 show equal amount of *HIST1H1E* cDNA, indicating stability of the mutant transcripts, which is consistent with the notion that intronless genes generally evade nonsense-mediated RNA decay. GAPDH is reported as internal control documenting the same use of template cDNA. (**B**) Chromatograms showing the heterozygous state of the two studied mutations as assayed on cDNA obtained from total RNA of fibroblasts from affected subjects S1 and S2. (**C**) Protein stability was assessed in COS-1 cells transiently transfected with wild-type Xpress-tagged *HIST1H1E* and mutants carrying the c.441dupC (p.Lys148Glnfs*48 [K148Qfs*48]) and c.464dupC (p.Lys157Glufs*39 [K157Efs*39]) mutations. After transfection (48 h), cells were treated with cycloheximide (CHX, 20 μg/ml) for the indicated time or left untreated. Protein levels was assessed by immunoblotting, using an anti-Xpress monoclonal antibody. GAPDH levels are shown to document equal loading of total proteins from cell lysates. Western blot from a representative experiment of three performed is shown.

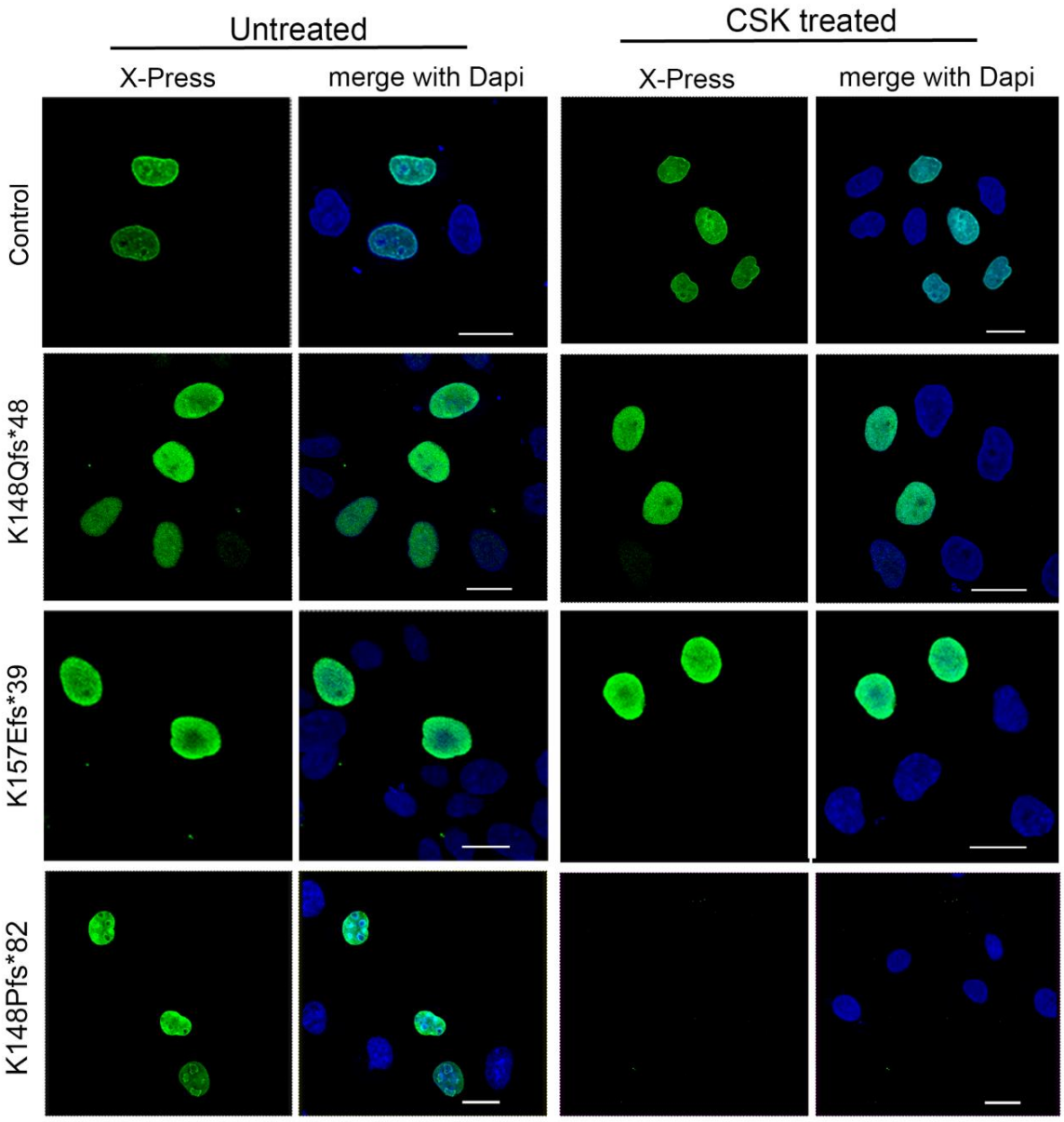

Figure S2. Disease-causing HIST1H1E mutants display proper subcellular localization and stably bind to chromatin. CLSM analyses were performed on HeLa cells transfected with vectors expressing Xpress-tagged wild-type HIST1H1E, two selected disease-causing mutants (p.Lys148Glnfs*48 [K148Qfs*48] and p.Lys157Glufs*39 [K157Efs*39]), and a HIST1H1E protein generated to express the third open reading frame at an equivalent position of the *C*-terminus (p.Lys148Profs*82 [K148Pfs*82]; not occurring in affected subjects). After 48 h from transfection, cells were treated with CSK (right) or left untreated (left), fixed, and stained (anti-X-press antibody). Nuclei were stained with DAPI (blue). Images show that, similarly to the wild-type protein, the disease-causing HIST1H1E mutants stably bind to chromatin. By contrast, the mutant carrying the alternative open reading frame was characterized by compromised chromatin binding, as shown by its loss of nuclear localization after CSK treatment. Bars correspond to 20 μm. Images are representative of > 200 analyzed cells.

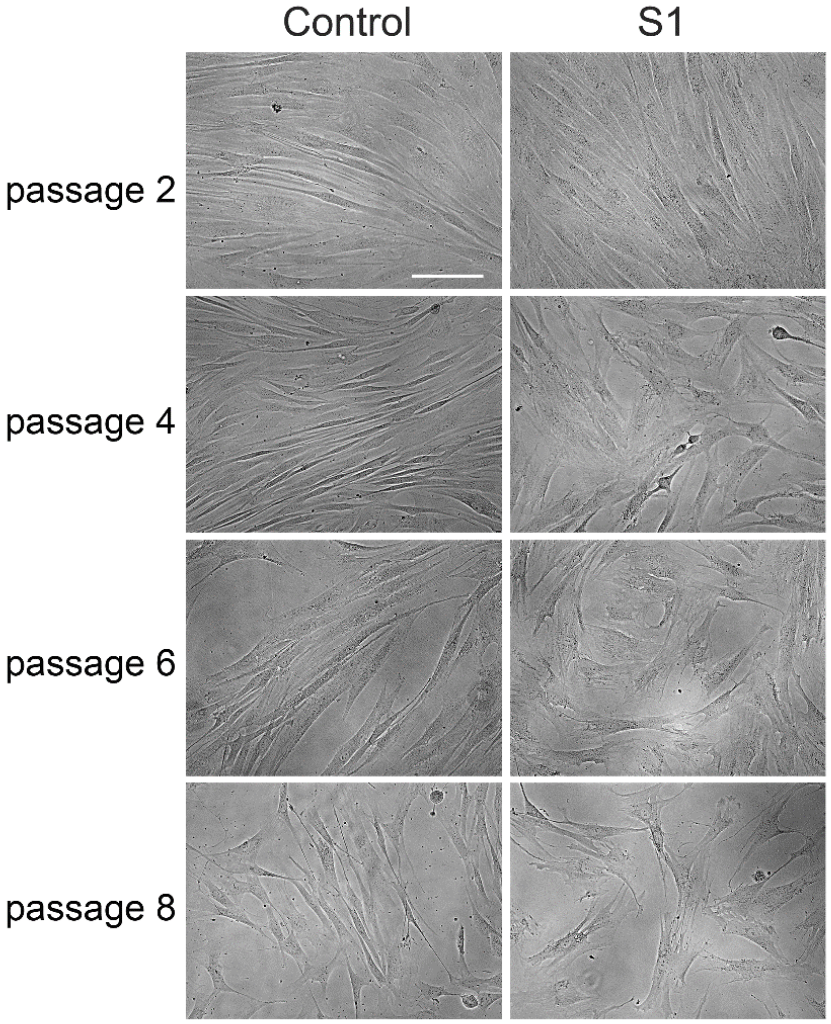

Figure S3. Accelerated cellular senescence in fibroblasts from affected subject S1. Images show morphological changes in cells endogenously expressing the heterozygous c.441dupC frameshift (p.Lys148Glnfs*48) in *HIST1H1E*. Morphology of cells rapidly progress from a thin and spindle shape to a large, flattened and irregular shape, which is visible since early passages. Photographs are at the same magnification (75 µm).

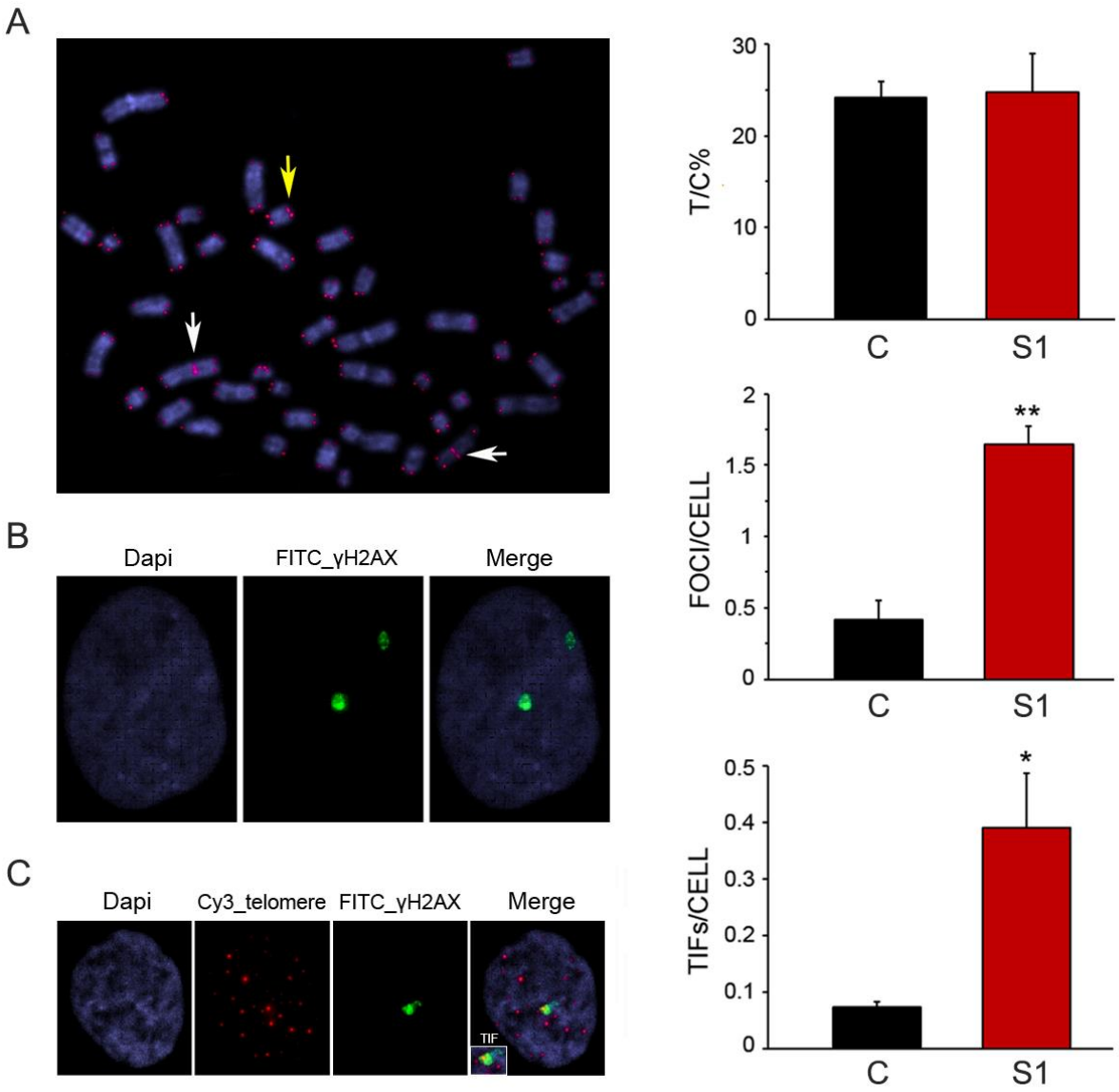

Figure S4. Telomere status and DNA damage sensitivity in fibroblasts from affected subject S1. (**A**) Q-FISH analysis. Representative image of a metaphase staining by Q-FISH (left). The yellow and white arrows indicate the telomeric signal and centromeres of chromosomes 2, respectively, which are used as internal reference in each metaphase. The telomere length was measured as the ratio between total telomeres fluorescence (T) and fluorescence of centromeres of chromosomes 2. The graph (mean ± SEM) shows no differences between control and S1 samples ($p < 0.05$, Mann-Whitney U test) (right). (**B**) Representative image of nuclei (DAPI) positive for γH2AX (green), a marker of DSBs (left). The graph shows the frequency of γH2AX foci per cell (mean ± SEM) (right). A significant increase in the frequency of foci was observed in S1 cells with respect to control cells (**$p < 0.001$; two-tailed Student's t-test). (**C**) Representative image of nuclei (DAPI) stained for γH2AX (green) and Cy3 (telomere-specific probe, red) (left). A magnification of telomere-γH2AX co-localisation (telomere dysfunction-induced foci, TIF) is also shown. The graph (mean ± SEM) shows the frequency of TIFs per cell (right), which occur with higher frequency in cells from subject S1 (*$p < 0.05$).

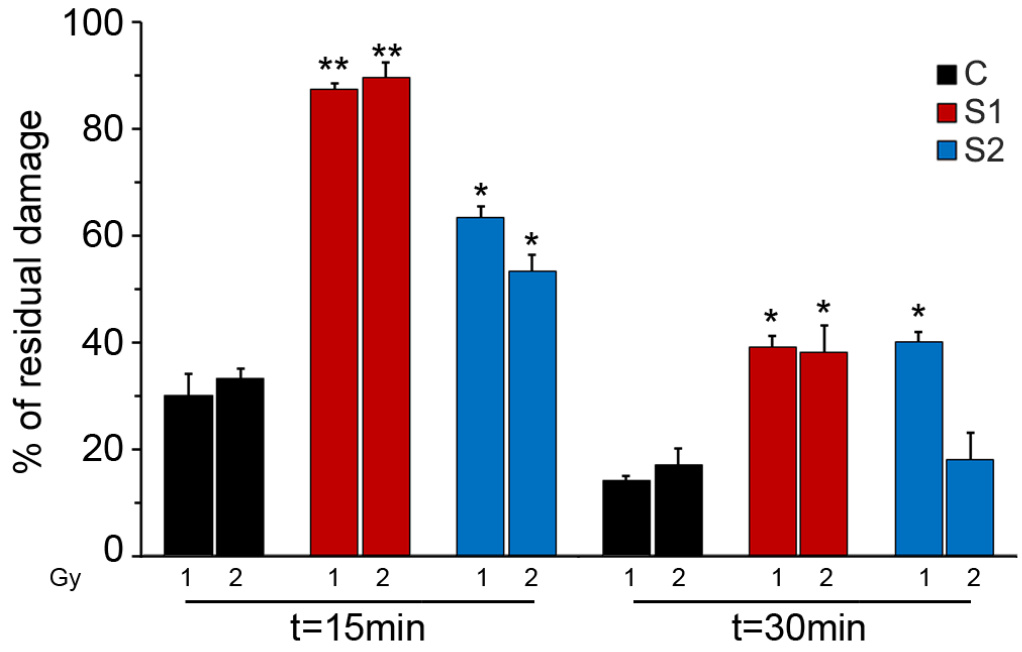

Figure S5. Defective HIST1H1E function is associated with defective/delayed DNA repair. DNA damage was induced by 1 or 2 Gy γ-ray irradiation. Following treatment, cells were incubated at 37 °C for 15 or 30 min to allow DNA repair. The percentage of residual DNA damage was calculated as follows: [(tail moment at time t after irradiation – basal tail moment)/(tail moment at t=0 – basal tail moment) × 100]. A lower/delayed capability to repair single/double strand breaks was observed in fibroblasts from affected subjects S1 and S2 compared to control cells (*p <0.02, **p < 0.001; two-tailed Student's t-test). For each experimental point, at least 75 cells were analyzed. Values are mean ± SEM of three independent experiments.

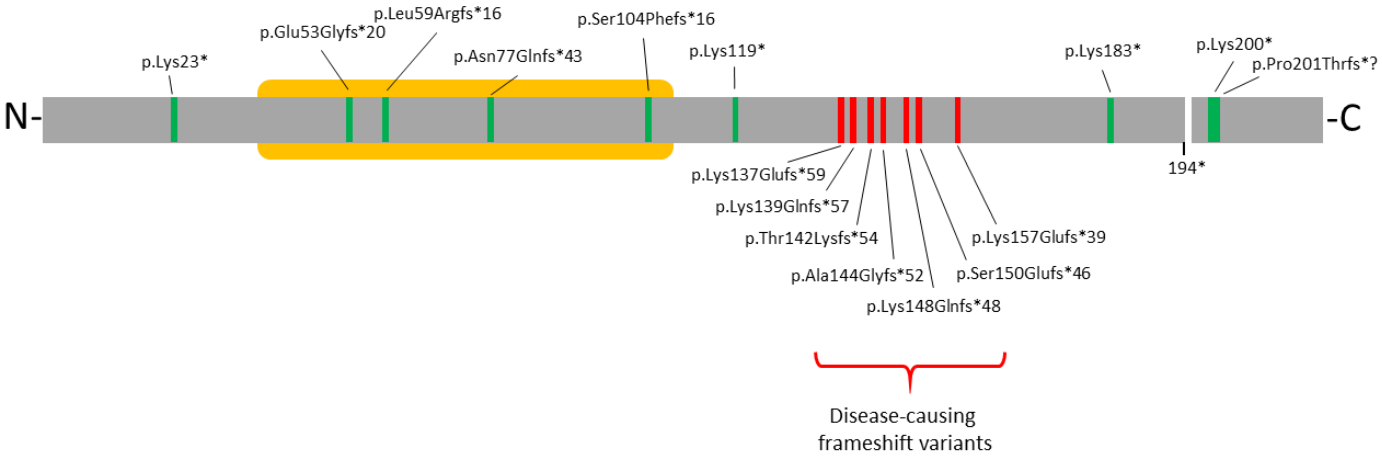

Figure S6. Truncating variants in *HIST1H1E*. Schematic diagram representing the HIST1H1E structure, and the position of the disease-causing frameshift mutations identified in this and previous studies (below the cartoon, red) and those reported in gnomAD (above the cartoon, green). The globular domain is shown in yellow. All disease-causing mutations result in a shorter protein with an identical divergent C-terminal tail (the new stop codon is shown below the cartoon, 194*). Differently, truncating mutations annotated in gnomAD either affect regions of the protein much more proximal to the N-terminus (the majority clustering within the globular domain) or are close to the C-terminus, downstream the regulatory serine/threonine residues. While the former are predicted to result in highly unstable proteins that likely undergo accelerated degradation and/or proteins unable to bind chromatin, the latter are expected to be loss-of-function mutants or behave as the wild-type protein, but are not expected to have a dominant negative effect.

SUPPLEMENTAL TABLES

Table S1. Predicted amino acid sequence of disease-causing frameshifts affecting the *C*-terminal region of HIST1H1E.

AA Change	AA Lenght	AA Sequence
Ref. Seq. (NP_005312.1)	219	MSETAPAAPAAPAPAEKTPVKKKARKSAGAAKRKASGPPVSELITKAVAASKERSGVSLAALKKALAAAGYDVEKNNSRIKLGLKSLVSKGTLVQTKGTGASGSFKLNKKA ASGEAKPKAKKAGAAKAKKPAGAAKKPKKATGAATPKKSAKKTPKKAKKPAAAAGAKKAKSPKKAKAAKPKKAPKSPAKAKAVKPKAAKPKTAKPKAAKPKKAAAKKK*
p.Lys137Glufs*59 (S12)	194	MSETAPAAPAAPAPAEKTPVKKKARKSAGAAKRKASGPPVSELITKAVAASKERSGVSLAALKKALAAAGYDVEKNNSRIKLGLKSLVSKGTLVQTKGTGASGSFKLNKKA ASGEAKPKAKKAGAAKAKKPAGAAKEAQEGDGGGHPQEERQEDPKEGEEAGCSCWSQKSEKPEKGESSQAKKGAQEPSEGQSS*
p.Lys139Glnfs*57 (S4, S6)	194	MSETAPAAPAAPAPAEKTPVKKKARKSAGAAKRKASGPPVSELITKAVAASKERSGVSLAALKKALAAAGYDVEKNNSRIKLGLKSLVSKGTLVQTKGTGASGSFKLNKKA ASGEAKPKAKKAGAAKAKKPAGAAKKPQEGDGGGHPQEERQEDPKEGEEAGCSCWSQKSEKPEKGESSQAKKGAQEPSEGQSS*
p.Thr142Lysfs*54 (S3, S9)	194	MSETAPAAPAAPAPAEKTPVKKKARKSAGAAKRKASGPPVSELITKAVAASKERSGVSLAALKKALAAAGYDVEKNNSRIKLGLKSLVSKGTLVQTKGTGASGSFKLNKKA ASGEAKPKAKKAGAAKAKKPAGAAKKPKKAKGVGHPQEERQEDPKEGEEAGCSCWSQKSEKPEKGESSQAKKGAQEPSEGQSS*
p.Ala144Glyfs*52 (S8, S13, S16, S20)	194	MSETAPAAPAAPAPAEKTPVKKKARKSAGAAKRKASGPPVSELITKAVAASKERSGVSLAALKKALAAAGYDVEKNNSRIKLGLKSLVSKGTLVQTKGTGASGSFKLNKKA ASGEAKPKAKKAGAAKAKKPAGAAKKPKKATGGGHPQEERQEDPKEGEEAGCSCWSQKSEKPEKGESSQAKKGAQEPSEGQSS*
p.Ala145Glyfs*51 (S15)	194	MSETAPAAPAAPAPAEKTPVKKKARKSAGAAKRKASGPPVSELITKAVAASKERSGVSLAALKKALAAAGYDVEKNNSRIKLGLKSLVSKGTLVQTKGTGASGSFKLNKKA ASGEAKPKAKKAGAAKAKKPAGAAKKPKKATGAGHPQEERQEDPKEGEEAGCSCWSQKSEKPEKGESSQAKKGAQEPSEGQSS*
p.Thr146Hisfs*50 (S14)	194	MSETAPAAPAAPAPAEKTPVKKKARKSAGAAKRKASGPPVSELITKAVAASKERSGVSLAALKKALAAAGYDVEKNNSRIKLGLKSLVSKGTLVQTKGTGASGSFKLNKKA ASGEAKPKAKKAGAAKAKKPAGAAKKPKKATGAAHPQEERQEDPKEGEEAGCSCWSQKSEKPEKGESSQAKKGAQEPSEGQSS*
p.Thr146Aspfs*42 (S19)	186	MSETAPAAPAAPAPAEKTPVKKKARKSAGAAKRKASGPPVSELITKAVAASKERSGVSLAALKKALAAAGYDVEKNNSRIKLGLKSLVSKGTLVQTKGTGASGSFKLNKKA ASGEAKPKAKKAGAAKAKKPAGAAKKPKKATGAADPKEGEEAGCSCWSQKSEKPEKGESSQAKKGAQEPSEGQSS*
p.Lys148Glnfs*48 (S1, S5, S10, S11, S17, S18)	194	MSETAPAAPAAPAPAEKTPVKKKARKSAGAAKRKASGPPVSELITKAVAASKERSGVSLAALKKALAAAGYDVEKNNSRIKLGLKSLVSKGTLVQTKGTGASGSFKLNKKA ASGEAKPKAKKAGAAKAKKPAGAAKKPKKATGAATPQEERQEDPKEGEEAGCSCWSQKSEKPEKGESSQAKKGAQEPSEGQSS*
p.Ser150Glufs*46 (S7)	194	MSETAPAAPAAPAPAEKTPVKKKARKSAGAAKRKASGPPVSELITKAVAASKERSGVSLAALKKALAAAGYDVEKNNSRIKLGLKSLVSKGTLVQTKGTGASGSFKLNKKA ASGEAKPKAKKAGAAKAKKPAGAAKKPKKATGAATPKKERQEDPKEGEEAGCSCWSQKSEKPEKGESSQAKKGAQEPSEGQSS*
p.Lys157Glufs*39 (S2)	194	MSETAPAAPAAPAPAEKTPVKKKARKSAGAAKRKASGPPVSELITKAVAASKERSGVSLAALKKALAAAGYDVEKNNSRIKLGLKSLVSKGTLVQTKGTGASGSFKLNKKA ASGEAKPKAKKAGAAKAKKPAGAAKKPKKATGAATPKKSAKKTPKEGEEAGCSCWSQKSEKPEKGESSQAKKGAQEPSEGQSS*
p.Lys148Profs*82 (frameshift not occurring in affected subjects)	228	MSETAPAAPAAPAPAEKTPVKKKARKSAGAAKRKASGPPVSELITKAVAASKERSGVSLAALKKALAAAGYDVEKNNSRIKLGLKSLVSKGTLVQTKGTGASGSFKLNKKA ASGEAKPKAKKAGAAKAKKPAGAAKKPKKATGAATPPRRAPRRPQRRRRSRLQLLEPKKRKARKRRKQPSQKRRPRAQRRPKQLNPRRLNQRPPSPRQPSQRRRQPRK SRKFLWPTA*

Table S2. Clinical features of the affected subjects with frameshift *HIST1H1E* mutations.

	Subject 1	Subject 2	Subject 3	Subject 4	Subject 5	Subject 6
Previously reported	-	-	-	-	-	-
Mutation						
cDNA (NM_005321.2)	c.441dupC	c.464dupC	c.425_431delinsAGGGGGTT	c.414dupC	c.441dupC	c.414dupC
Protein change *(www.mutalyzer.nl)*	p.Lys148Glnfs*48	p.Lys157Glufs*39	p.Thr142Lysfs*54	p.Lys139Glnfs*57	p.Lys148Glnfs*48	p.Lys139Glnfs*57
De novo inheritance	+	+	+	+	+	U
Epidemiology						
Origin	caucasian	caucasian	caucasian	caucasian	caucasian	african american
Gender	male	female	male	female	female	female
Age (years) at last observation	49y	4y 6m	30y 9m	14m	12y	3y
Duration gestation (weeks)	U	40w	38w	38w	41w	39w
Pregnancy	uneventful	late hyperemesis	decreased fetal movement	wide ventricles seen on ultrasound	uneventful, amniocentesis was performed	uneventful
Neonatal problems	U	-	fetal heart decelerations. Apgar 4 and 6, cyanosis at birth, intubation for ventilation (NICU)	primary cesarean (1st pregnancy breech position)	-	congenital hypotonia, feeding difficulties, FTT
Birth Weight, g (SD)	U	3714g (+0.73SD)	3713.8g (+0,4SD)	4470g (+2.75SD)	3150g (-0.41SD)	3573g (+0.45SD)
Birth Length, cm (SD)	U	53.3cm (+1.8SD)	52.1cm (+1SD)	U	49.5cm (-0.2SD)	53.3 cm (+1.8SD)
Birth OFC, cm (SD)	U	U	35 cm (+0.1 SD)	U	33cm (-1.32SD)	35 cm (+0.1SD)
Weight at last observation, kg (SD)	U	21 kg (+1.93SD)	59 kg (+0.09SD)	10.3 kg (+1.54SD)	41.6 kg (-0.02SD)	14.1 kg (0.14SD)
Height at last observation, cm (SD)	U	111 cm (+1.83SD)	167.2 cm (+0.62SD)	74 cm (+0.56SD)	146.2 cm (-0.74SD)	91.4 cm (-0.96SD)
OFC at last observation, cm (SD)	U	53.8 cm (+2.1SD)	60cm (+3.4SD)	50 cm (+3.48SD)	54.9 cm (+1.14SD) (+2SD at age 4, while length -0,5SD)	49.2 cm (-0.07SD)
Growth						
Delay/ ID : mild=1; moderate=2; severe=3, unspecified	2	1	1	0	1	2
Sitting unsupported (months)	U	10	8	8.5	12	6
Walking independently (months)	U	16	24	not yet at age 14m, but makes steps holding table since age 1 year	30	24
Motor delay	+	+	+	seems late but still within range	+	+
Speech delay	+	+	+	U	+	+
Hypotonia	U	-	+	+	-	+
Seizures, type and treatment	U	childhood focal seizures	febrile seizures	-	-	-
Hearing loss	+	-	+	-	-	+
Frequent otitis media	U	-	+	-	-	+
Eye defects	U	U	+	-	+	+
Hypermetropia (H)/ myopia (M)	U	-	M	-	H	-
Astigmatism	U	-	-	-	+	+ - simple hyperopic
Strabismus	U	-	+	-	+	-

	Subject 1	Subject 2	Subject 3	Subject 4	Subject 5	Subject 6
Craniofacial features						
Coarse face	U	-	-	-	-	-
High hairline	+	+	+	+	+	+
Abnormal hair	sparse hair, generalized hypopigmentation of hair, hypotrichosis	frontal upsweep, thin, sparse hair	alopecia totalis (sparse frontotemporal hair) and sparse eyelashes since age 10y; delayed hair growth as child; no eyebrows until about age 4.	sparse hair	thin hair, Widow's peak (like father)	-
Prominent forehead	+	+	+	+	+	+
Bitemporal narrowing	+	U	+	+	U	U
Epicanthus/telecanthus	epicanthus	U	U	U	U	U
Downward slant palpebral fissures	U (small)	+	+	- (narrow)	+ (narrow)	+
Deepset eyes	U	U	+	U	U	U
Ptosis	+	-	+	-	-	-
Hypertelorism	+	-	U	+	+++	+
Small/pointed chin	U	+	+	+	-	-
Nasal bridge anomalies	narrow nasal bridge	wide, low and flat	U	wide	-	wide
Upturned nasal tip	U	+	-	-	-	-
Full nasal tip	U	+	+	+	-	+
Thick alae nasi	U	+	+	+	-	+
Short nose	U	-	-	-	-	-
Prominent cheek bones	U	U	+	U	U	U
Smooth philtrum	U	+	U	-	-	-
Broad philtrum	U	-	U	-	-	-
Long philtrum	U	+	U	-	-	+
Mouth abnormalities	U	thin upper vermillion	U	thin upper vermillion	accentuated Cupid's bow, high palate	-
Micrognathia	+	U	+	U	U	U
Widely spaced teeth	U	-	U	U	widely spaced central incisors	U
Enlarged tongue	U	U	+	-	U	U
Ear abnormalities	low set	thickening of superior scaphohelices	low set, upturned ear lobes	-	low set, simple helix, upturned ear lobes	-
Hand abnormalities	brachydactyly, broad thumbs, deep palmar crease	-	bilaterally brachydactyly (shortening of distal phalangeal area), unilateral palmar crease	-	tapering fingers, slightly shorter 4th metacarpals. Camptodactyly. Palmar erythema, low-set thumbs	-
Joint hyperlaxity/stiffness	U	-	U	U	very stiff fingers	-
Nail anomalies	nail dysplasia	-	middle ridges on his two thumbnails	-	thin and short nails	-
Feet abnormalities (flat feet, sandal gap,...)	U	-	orthopedic insoles, flat feet	-	orthopedic insoles, stiff feet, plantar erythema	-
Toe abnormalities	broad hallux, deviation of hallux	broad toes	U	-	long halluces	-
RX abnormalities	U	-	-	U	osteopenia, advanced bone age, multiple small stress fractures	-
Other limb abnormalities	U	-	U	-	lower limb pitting edema, genua valga, slight leg lenght difference	-

	Subject 1	Subject 2	Subject 3	Subject 4	Subject 5	Subject 6
Other						
Skull abnormalities	dolichocephaly (scaphocephaly), abnormal skull ossification	dolichocephaly	macrocephaly	mild turricephaly	scaphocephaly	-
Cryptorchidism	U	-	unilateral	-	-	-
Renal abnormalities	U	U	kidney cysts bilaterally	U	U	U
Skin	multiple nevi, skin hyperpigmentation, cutis laxa	1 hypopigmented lesion on the left knee	cutis marmorata when young.	-	mild cutis marmorata, dry skin, multiple lentigines solaris in face	-
Scoliosis (mild, severe)	U	-	U	-	mild	mild
Widely spaced/inverted nipples	U	-	U	-	+	-
Cardiac abnormalities	-	-	-	small 'atrial septum defect	-	-
Pectus excavatum/carinatum	excavatum, scapular wings	-	U	-	excavatum	-
dentition (normal; pointed; delayed prim / delayed permanent/missing permanent)	U	early loss of primary teeth/delayed permanent teeth	small, poorly enameled teeth	pointed teeth	small, pointed teeth, some permanent teeth missing, short roots	U
sleep problems	U	+ (restless sleeper and early awake)	U	-	'+ (frequently awake during night, early awake)	-
Laboratory abnormalities	pancytopenia (possible autoimmune origin), autoimmune disorder (systemic lupus erythematosus), congenital hypothyroidism	mildly elevated creatine (age 2 1/2)	low hemoglobin (iron supplementation ongoing)	-	Hypophosphatasia (zinc deficiency)	-
Neuroradiology				cerebral ultrasound at 6m: mild ventricular enlargement		
MRI brain (at age in months)	-	approx 2y 6m	CT scan at 4 m of age and 6 y normal	-	U	9m
MRI brain abnormality	U	mild ventricular enlargement	U	U	-	mild inferior vermian hypoplasia
Autism/Behavioral problems	abnormal behavior, psychotic episodes	autism spectrum disorder	U	U	diminished eye contact in childhood and socialization anomalies	-
Clinical diagnosis/tested for:	U	Clinical suspicion of Sotos syndrome NSD1 on WES normal, CMA normal	Clinical suspicion of Sotos syndrome NSD1 gene normal. FXS, Pallister-Killian syndrome, Prader Willi syndrome, Smith Magenis syndrome screening normal	SNP array normal; WES panel overgrowth syndromes	Clinical suspicion of Sotos syndrome NSD1 gene normal	U

	Subject 7	Subject 8	Subject 9	Subject 10	Subject 11	Subject 12	Subject 13
Previously reported	-	-	-	-	-	-	-
Mutation							
cDNA (NM_005321.2)	c.447dupG	c.430dupG	c.425delinsAG	c.441dupC	c.441dupC	c.408dupG	c.430dupG
Protein change *(www.mutalyzer.nl)*	p.Ser150Glufs*46	p.Ala144Glyfs*52	p.Thr142Lysfs*54	p.Lys148Glnfs*48	p.Lys148Glnfs*48	p.Lys137Glufs*59	p.A144Gfs*53
De novo inheritance	+	U	U	+	+	+	+
Epidemiology							
Origin	caucasian	asian	caucasian	caucasian	caucasian	caucasian	caucasian
Gender	male	male	female	male	female	male	female
Age (years) at last observation	11y 11m	4y 9m	2y	1y 7m	6y	4y	17m
Duration gestation (weeks)	34w	at term	at term	39w	40+2w	39w	39w
Pregnancy	ultrasound diagnosis of macrocephaly (32 weeks)	U	U	uneventful	uneventful	uneventful	uneventful
Neonatal problems	3 weeks in NICU	U	U	-	Apgar 6-9-9, insufflation breaths and PEEP. Ventilatory assistance 4 days after birth	-	primary cesarean (1st pregnancy breech position)
Birth Weight, g (SD)	2600g (-1.75SD)	3400g (0SD)	U	4100g (+1.4SD)	3482g (+0.27SD)	3886g (+1.05SD)	3780g (SD +0.81SD)
Birth Length, cm (SD)	51 cm (0SD)	U	U	55 cm (+2.7SD)	U	55 cm (+2.7SD)	50.8 cm (+0.59SD)
Birth OFC, cm (SD)	35 cm (+0.1 SD)	U	U	39cm (+3.0SD)	U	35 cm (+0.1SD)	38 cm (SD +1.82SD)
Weight at last observation, kg (SD)	37.7 kg (-0.44SD)	21.5 kg (+1.29SD)	13.3 kg (+1.16SD)	15 kg (+2.8SD)	26.2 kg (+1.65SD)	21.5 kg (+2.11SD)	9.995 kg (-0.88SD)
Height at last observation, cm (SD)	139.7 cm (-1.62SD)	109.8 cm (+0.43SD)	86 cm (+0.08SD)	92.5 cm (+3.65SD)	120.2 cm (+0.99SD)	106 cm (+0.64SD)	77.1 cm (-0.93SD)
OFC at last observation, cm (SD)	58.8 cm (+3.98SD)	55 cm (+3.53SD)	49.4 cm (+1.07SD)	47.3 cm (+0.41SD)	56 cm (+2.94SD) at age 6y 9m	56 cm (+3.68SD)	50.7 cm (+3.19SD)
Growth							
Delay/ ID : mild=1; moderate=2; severe=3, unspecified	2	0	unspecified	2	2	1	2
Sitting unsupported (months)	12	11	U	8	14	9	9
Walking independently (months)	30	30	U	not yet at 2y 9m, can make steps with support	66	15	not yet but crawling
Motor delay	+	+	U	+	+	+	+
Speech delay	+	+	U	+	+	+	+
Hypotonia	+	+	U	-	+	+	+
Seizures, type and treatment	single childhood seizure	U	febrile seizures	febrile	recurrent status epilepticus, valproate treatment	-	-
Hearing loss	-	U	+	-	-	-	bilateral mild to moderate sensorineural hearing loss
Frequent otitis media	+	U	U	-	-	- (two times)	-
Eye defects	+	+	U	U	+	lacrimal duct stenosis (operation at 1.5y)	+
Hypermetropia (H)/ myopia (M)	M	U	U	-	H	-	M
Astigmatism	+	U	U	-	-	-	+
Strabismus	-	+	U	-	+ (exotropia)	-	-

	Subject 7	Subject 8	Subject 9	Subject 10	Subject 11	Subject 12	Subject 13
Craniofacial features							
Coarse face	-	U	U	+	+	+	+
High hairline	+	+	U	+	+	+	+
Abnormal hair	-	U	U	-	thin hair	-	-
Prominent forehead	+	+	+	+	+	+	+
Bitemporal narrowing	U	U	U	U	U	U	+
Epicanthus/telecanthus	U	epicanthus	epicanthus	U	U	-	+
Downward slant palpebral fissures	-	+	U	+ (accentuated by puffy eyelids)	-	-	+
Deepset eyes	U	U	+	U	U	+	-
Ptosis	-	U	U	-	-	-	+ (mild)
Hypertelorism	+	U	U	+	+	+	+
Small/pointed chin	-	U	U	-	-	-	+
Nasal bridge anomalies	-	wide	wide	wide	wide	wide	-
Upturned nasal tip	-	+	U	-	+	-	+
Full nasal tip	+	U	+	+	+	+	+
Thick alae nasi	-	U	U	-	-	+	+
Short nose	-	U	U	-	-	-	+
Prominent cheek bones	U	U	U	U	U	-	-
Smooth philtrum	-	U	U	-	-	-	-
Broad philtrum	-	U	U	-	-	-	-
Long philtrum	-	U	U	-	-	-	+
Mouth abnormalities	thin upper vermillion	U	U	-	-	thin upper vermillion, thick lower vermillion, drooping lower lip	thin upper vermillion
Micrognathia	U	U	U	U	U	-	-
Widely spaced teeth	-	U	U	+	U	+	-
Enlarged tongue	U	U	U	U	U	-	-
Ear abnormalities	low set	U	low set	low set, protruding	-	low set, rotated ears	low set, posteriorly rotated
Hand abnormalities	-	tapering fingers, 5th finger clinodactyly, bilateral single palmar crease	U	tapering fingers, broad thumbs	small hands	relatively large hands	single transverse palmer creases
Joint hyperlaxity/stiffness	-	U	U	-	-	-	+
Nail anomalies	-	U	U	-	-	flaky nails	-
Feet abnormalities (flat feet, sandal gap,...)	-	bilateral pes planus	U	-	orthopedic insoles	-	-
Toe abnormalities	-	5th toe overlaps 4th toe	U	-	U	relatively large feet	overlapping toes
RX abnormalities	advanced bone age	-	U	U	-	advanced bone age	scoliosis
Other limb abnormalities	-	U	U	-	valgus hips	-	hip dysplasia

	Subject 7	Subject 8	Subject 9	Subject 10	Subject 11	Subject 12	Subject 13
Other					hemangioma leg		gastroesophageal reflux disease
Skull abnormalities	-	U	U	scaphocephaly	scaphocephaly	U	dolichocephaly with patent sagittal suture
Cryptorchidism	bilateral	U	-	bilateral	-	+	-
Renal abnormalities	U	U	U	U	U	U	U
Skin	-	flat hyperpigmented patches on abdomen and thighs (dad attributes to post viral infection)	U	-	-	mild cutis laxa in abdominal area	-
Scoliosis (mild, severe)	-	U	U	-	-	-	mild
Widely spaced/inverted nipples	-	U	U	-	-	+	
Cardiac abnormalities	-	U	U	-	-	atrial septum defect	small atrial septum defect
Pectus excavatum/carinatum	-	U	U	-	-	-	-
dentition (normal; pointed; delayed prim / delayed permanent/missing permanent)	crowded teeth	U	U	small teeth, widely spaced	tooth dysgenesia with extreme short radices of milk molars with 4 elementes missing	early eruption of teeth	high arched palate
sleep problems	-	U	U	-	U	-	-
Laboratory abnormalities	-	U	U	-	-	-	-
Neuroradiology						-	
MRI brain (at age in months)	3 y; repeat 5y	U	U	12 m	5m	U	14m
MRI brain abnormality	partial agenesis of corpus callosum	periventricular white matter abnormality	U	arachnoid cyst	cavum septum pellucidum	U	Mild prominence of the subarachnoid fluid spaces
Autism/Behavioral problems	ADHD	self-stimulatory behaviors	U	stereotypic movements with hands, rolls with eyes when tired	-	-	none at 17m
Clinical diagnosis/tested for:	U	U	U	CMA and metabolic screening normal	Clinical suspicion of Sotos syndrome NSD1, PTEN and EZH2 genes normal, FXS normal, CMA normal	Clinical suspicion of Simpson-Golabi-Behmel syndrome; CMA, metabolic screening, FXS and gene panel normal	Rasopthay panel normal; SNP array normal; WES

	Subject 14	**Subject 15**	**Subject 16**	**Subject 17**	**Subject 18**	**Subject 19**	**Subject 20**
Previously reported	*Duffney et al. 2018*	*Takenouchi et al. 2018*	*Tatton-Brown et al. 2017*	*Tatton-Brown et al. 2017*	*Tatton-Brown et al. 2017*	*Tatton-Brown et al. 2017*	*Tatton-Brown et al. 2017*
Mutation							
cDNA (NM_005321.2)	c.435dupC	c.433dup	c.430dupG	c.441dupC	c.441dupC	c.436_458del23	c.430dupG
Protein change *(www.mutalyzer.nl)*	p.Thr146Hisfs*50	p.Ala145Glyfs*51	p.Ala144Glyfs*52	p.Lys148Glnfs*48	p.Lys148Glnfs*48	p.Thr146Aspfs*42	p.Ala144Glyfs*52
De novo inheritance	+	+	+	+	U	+	+
Epidemiology							
Origin	caucasian	asian	caucasian	caucasian	U	U	caucasian
Gender	male	female	female	male	female	female	male
Age (years) at last observation	10y	21y	13y	15y 6m	4y 3m	1y 10m	8y 6m
Duration gestation (weeks)	38w	36w	at term	41w	at term	37w	41w
Pregnancy	early delivery (maternal car accident at 38 weeks)	U	U	uneventful	U	uneventful	complicated by exposure to chicken pox
Neonatal problems	2 weeks in NICU, jaundice, micrognathia increased muscle tone and feeding difficulties	U	congenital hypotonia	congenital hypotonia, feeding difficulties	congenital hypotonia, feeding difficulties	hypoglycemia and increased muscle tone	U
Birth Weight, g (SD)	3200g (-0.3SD)	2876g (+1.6SD)	3580g (+0.47SD)	4750g (+2.4SD)	4790g (+2.62SD)	3250g (+0.8SD)	3740g (+0.78SD)
Birth Length, cm (SD)	49.5cm (-0.2SD)	49cm (+1.4SD)	53cm (+1.65SD)	U	57cm (+3.76SD)	49cm (+0.7SD)	U
Birth OFC, cm (SD)	U	33.4 cm (+0.9SD)	U	U	U	37cm (+3.3SD)	U
Weight at last observation, kg (SD)	54.5 kg (+2.66SD)	U	48.8 kg (+0.4SD)	U	24 kg (+2.45SD)	12 kg (+0.65SD)	33 kg (+1.34SD)
Height at last observation, cm (SD)	144.8 cm (+0.96SD)	151.8 cm (-1.74SD)	150.8 cm (-0.8SD)	166.5 cm (-0.6SD)	108 cm (+0.8SD)	85 cm (+0.12SD)	133.2 cm (+0.56SD)
OFC at last observation, cm (SD)	53 cm (+0.25SD)	54.4 cm (-0.15SD; relative macrocephaly)	55.8 cm (+1.57SD)	58.7 cm (+2.03SD)	55 cm (+3.78SD)	51 cm (+2.65SD)	59 cm (+4.92SD) at age 6,3
Growth							
Delay/ ID : mild=1; moderate=2; severe=3, unspecified	2	3	1	2	unspecified	2	3
Sitting unsupported (months)	9	U	U	U	U	U	U
Walking independently (months)	24	30	U	U	U	U	U
Motor delay	+	U	U	U	U	U	U
Speech delay	+	+	U	U	U	U	+
Hypotonia	-	U	+	+	+	U	U
Seizures, type and treatment	single childhood seizure	U	U	U	U	U	U
Hearing loss	-	U	U	U	U	U	-
Frequent otitis media	-	U	U	U	U	U	U
Eye defects	U	cataracts at age 21y	U	U	U	U	delayed visual maturation
Hypermetropia (H)/ myopia (M)	-	U	U	U	U	U	U
Astigmatism	+	U	U	U	U	U	+
Strabismus	+	+	+	U	U	U	left amblyopia

	Subject 14	Subject 15	Subject 16	Subject 17	Subject 18	Subject 19	Subject 20
Craniofacial features							
Coarse face	-	U	U	U	U	U	U
High hairline	-	+	+	U	U	U	U
Abnormal hair	-	U	U	U	U	U	U
Prominent forehead	-	U	U	U	U	U	U
Bitemporal narrowing	U	U	U	U	U	U	U
Epicanthus/telecanthus	U	epicanthus	telecanthus	U	U	U	U
Downward slant palpebral fissures	+	U (short)	U	U	U	U	U
Deepset eyes	U	U	U	U	U	U	U
Ptosis	-	U	U	U	U	U	U
Hypertelorism	+	U	U	U	U	U	U
Small/pointed chin	+	U	U	U	U	U	U
Nasal bridge anomalies	low	wide	U	U	U	U	U
Upturned nasal tip	-	U	U	U	U	U	U
Full nasal tip	-	U	U	U	U	U	U
Thick alae nasi	-	U	U	U	U	U	U
Short nose	-	U	U	U	U	U	U
Prominent cheek bones	U	+	U	U	U	U	U
Smooth philtrum	+	U	U	U	U	U	U
Broad philtrum	+	U	U	U	U	U	U
Long philtrum	+	+	U	U	U	U	U
Mouth abnormalities	accentuated Cupid's bow	high-arched, wide uvula	U	U	U	U	U
Micrognathia	+	U	U	U	U	U	U
Widely spaced teeth	-	U	U	U	U	U	U
Enlarged tongue	U	U	U	U	U	U	U
Ear abnormalities	-	simple auricles	U	U	U	U	U
Hand abnormalities	clinodactyly for 5th fingers	bilateral 5th finger clinodactyly	U	U	U	camptodactyly	U
Joint hyperlaxity/stiffness	+	U	U	U	U	U	U
Nail anomalies	+, nail hypoplasia	U	U	dry, flaky nails	U	U	U
Feet abnormalities (flat feet, sandal gap,...)	pes planus	U	U	U	U	U	talipes equi-varus
Toe abnormalities	long halluces	U	U	U	U	U	U
RX abnormalities	multiple small stress fractures	U	advanced bone age	U	U	U	U
Other limb abnormalities	-	U	U	U	U	U	U

	Subject 14	Subject 15	Subject 16	Subject 17	Subject 18	Subject 19	Subject 20
Other							
Skull abnormalities	-	U	U	U	U	U	U
Cryptorchidism	-	U	-	bilateral	U	U	U
Renal abnormalities	U	U	U	U	U	U	U
Skin	-	hyperkeratosis, multiple lentigines	U	multiple nevi, redundant skin on palm of hands	U	U	U
Scoliosis (mild, severe)	severe	U	severe	U	U	U	U
Widely spaced/inverted nipples	+	inverted nipples	U	U	U	U	U
Cardiac abnormalities	-	U	U	U	U	U	U
Pectus excavatum/carinatum	-	U	U	U	U	U	U
dentition (normal; pointed; delayed prim / delayed permanent/missing permanent)	multiple caries	U	U	major dental problems with crumbling teeth	U	U	U
sleep problems	'+ (staying asleep, gets up at night and can't go back to sleep)	U	U	U	U	U	U
Laboratory abnormalities	U	diabetes mellitus	U	U	U	U	U
Neuroradiology							
MRI brain (at age in months)	24m	U	4m	U	U	U	U
MRI brain abnormality	arachnoid cyst and mild hydrocephalus	U	mild ventricular enlargement	U	U	U	thin corpus callosum and periventricular leukomalacia
Autism/Behavioral problems	lack of eye contact, ADHD, obsessive behaviors with fixated interest	auditory hypersensitivity, high pitched voice	U	anxiety disorder refractory to medical treatment, developed phobias	U	U	challenging behavior
Clinical diagnosis/tested for:	SHANK3 related disorder and FXS screening normal, CMA normal	U	U	U	U	Clinical suspicion of Weaver syndrome	U

Table S3. Aging signs/features of the affected subjects with frameshift *HIST1H1E* mutations. The table includes the subjects included in the present study (S1 to S13) and those previously reported in the literature (S14 to S20).

	S1	**S2**	**S3**	**S4**	**S5**	**S6**	**S7**	**S8**	**S9**	**S10**	**S11**	**S12**	**S13**	**S14**	**S15**	**S16**	**S17**	**S18**	**S19**	**S20**	**N**
Age (years)	49	4.5	30.7	1.2	12	3	11.9	4.7	2	1.6	6	4	1.4	10	21	13	15.5	4.2	1.9	8.5	20
Hypotrichosis	Y	Y	Y	Y	Y						Y										6
Skin hyperpigmentation	Y				Y			Y							Y		Y				5
Hyperkeratosis															Y						1
Dry skin					Y										Y						2
Cutis laxa	Y											Y					Y				3
Cutis marmorata		Y	Y		Y																3
Nail abnormalities			Y		Y							Y					Y				4
Dental problems		Y	Y		Y							Y		Y			Y				6
Osteopenia					Y																1
Limb fractures					Y									Y							2
Advanced bone age					Y		Y					Y				Y					4
Joint stiffness					Y								Y	Y							3
Lower limb pitting edema					Y																1
Hearing loss	Y		Y										Y								3
Cataracts															Y						1
Ptosis	Y		Y										Y								3
Diabetes Mellitus															Y						1
Pancytopenia/autoimmune disorder (systemic lupus erythematosus)	Y																				1

Table S4. List of the CpG sites located in the promoter regions (200-1500 bp from transcription start sites, TSS) of genes found to be differentially methylated in affected individuals with *HIST1H1E* mutations and controls.

IlmnID	CHR	MAPINFO	UCSC RefGene Name	UCSC RefGene Group	mean controls	mean Pt1	mean other patients
cg25880954	1	47900630	MGC12982;FOXD2	TSS1500;TSS1500	0.78	0.91	0.81
cg04863005	1	59043208	TACSTD2	TSS200	0.39	0.09	0.31
cg15100762	1	66516476	LOC101927139;PDE4B;PDE4B; PDE4B;PDE4B;PDE4B	TSS200;Body;Body;Body;Body; Body	0.85	0.93	0.95
cg09408571	1	101003634	GPR88	TSS200	0.63	0.79	0.72
cg06223162	1	101003688	GPR88	TSS200	0.46	0.54	0.43
cg16180556	1	110230269	GSTM1;GSTM1	TSS200;TSS200	0.29	0.28	0.52
cg24506221	1	110230401	GSTM1;GSTM1	TSS200;TSS200	0.24	0.38	0.48
cg20803293	1	110254709	GSTM5	TSS200	0.35	0.27	0.51
cg16810724	1	110752159	KCNC4-AS1;KCNC4;KCNC4;KCNC4	Body;TSS1500;TSS1500;TSS1500	0.62	0.64	0.49
cg06205333	1	112161618	RAP1A;RAP1A	TSS1500;TSS1500	0.61	0.82	0.48
cg10185505	1	150335496	RPRD2;RPRD2;RPRD2	TSS1500;TSS1500;TSS1500	0.72	0.54	0.56
cg12650227	1	152572930	LCE3C	TSS1500	0.61	0.19	0.56
cg08477332	1	153590243	S100A14	TSS1500	0.35	0.43	0.45
cg23216745	1	154929762	PBXIP1;PYGO2	TSS1500;3'UTR	0.82	0.89	0.90
cg27003165	1	162381929	SH2D1B	TSS200	0.52	0.40	0.67
cg13124890	1	162382662	SH2D1B	TSS1500	0.49	0.28	0.67
cg01062020	1	162382848	SH2D1B	TSS1500	0.32	0.08	0.47
cg19368440	1	164744070	LOC100505795;PBX1;PBX1;PBX1	TSS200;Body;Body;Body	0.32	0.55	0.79
cg07533224	1	205819345	PM20D1	TSS200	0.43	0.52	0.48
cg12898220	1	205819356	PM20D1	TSS200	0.48	0.57	0.51
cg05841700	1	205819383	PM20D1	TSS200	0.36	0.30	0.37
cg11965913	1	205819406	PM20D1	TSS200	0.26	0.25	0.28
cg07167872	1	205819463	PM20D1	TSS200	0.36	0.42	0.34
cg24503407	1	205819492	PM20D1	TSS1500	0.37	0.46	0.40
cg16334093	1	205819600	PM20D1	TSS1500	0.49	0.51	0.53
cg07157834	1	205819609	PM20D1	TSS1500	0.53	0.57	0.62
cg00541777	2	3652840	COLEC11;COLEC11;COLEC11;COLEC11; COLEC11;COLEC11;COLEC11;COLEC11; COLEC11;COLEC11;COLEC11	TSS1500;TSS1500;TSS1500;TSS1500; Body;Body;Body;Body;Body;Body; Body	0.73	0.66	0.81
cg10326673	2	30669757	LCLAT1;LCLAT1;LCLAT1;LCLAT1	TSS1500;TSS1500;TSS1500;TSS1500	0.23	0.50	0.42
cg15652532	2	30669759	LCLAT1;LCLAT1	TSS1500;TSS1500	0.23	0.52	0.39
cg24521141	2	38744309	LOC101929596	TSS1500	0.78	0.95	0.89
cg05043910	2	99872119	LYG2	TSS1500	0.52	0.53	0.60
cg23122642	2	113992694	PAX8-AS1;PAX8-AS1;PAX8;PAX8; PAX8;PAX8	TSS1500;TSS1500;Body;Body;Body; Body	0.61	0.52	0.58
cg21482265	2	113992762	PAX8;PAX8;PAX8;PAX8;PAX8;LOC440 839;LOC654433	Body;Body;Body;Body;Body;Body; TSS1500	0.67	0.61	0.68
cg19083407	2	113993142	PAX8;PAX8;PAX8;PAX8;PAX8; LOC440839;LOC654433	Body;Body;Body;Body;Body;Body; TSS1500	0.59	0.57	0.57
cg08010094	2	139539001	NXPH2	TSS1500	0.52	0.18	0.38
cg19840088	2	149894678	LYPD6B	TSS1500	0.60	0.93	0.64
cg20351137	2	177133606	MTX2;MTX2	TSS1500;TSS1500	0.63	0.67	0.49
cg16955800	2	183981465	NUP35	TSS1500	0.34	0.45	0.21
cg20517941	2	201600636	LOC100507140;AOX2P	TSS1500;Body	0.22	0.39	0.33
cg21893210	2	220108407	GLB1L;GLB1L;GLB1L	5'UTR;5'UTR;TSS200	0.39	0.49	0.20
cg24061197	2	220108496	GLB1L;GLB1L;GLB1L	5'UTR;5'UTR;TSS200	0.42	0.59	0.27
cg01588581	2	241832900	C2orf54;C2orf54	TSS1500;Body	0.50	0.41	0.55
cg01904194	2	241832904	C2orf54;C2orf54;C2orf54	TSS1500;TSS1500;Body	0.60	0.45	0.62
cg08144588	3	3080327	CNTN4;CNTN4;CNTN4	Body;TSS1500;Body	0.81	0.94	0.75
cg00457450	3	15107267	MRPS25	TSS1500	0.74	0.30	0.38
cg08033130	3	45983597	CXCR6;FYCO1	TSS1500;Body	0.43	0.34	0.56
cg20540428	3	73045686	PPP4R2	TSS1500	0.35	0.20	0.51
cg06085042	3	195425033	MIR570	TSS1500	0.59	0.50	0.66
cg15727583	3	196757701	MFI2;MFI2	TSS1500;TSS1500	0.77	0.97	0.85
cg01132407	4	645781	PDE6B;PDE6B;PDE6B	TSS1500;Body;Body	0.65	0.85	0.50
cg19247841	4	48485301	SLC10A4	TSS200	0.11	0.53	0.08
cg19978674	4	57523826	HOPX;HOPX;HOPX;HOPX;HOPX	5'UTR;Body;Body;TSS1500;TSS1500	0.35	0.21	0.64

cg07952421	4	69435601	UGT2B15;UGT2B17	TSS1500;TSS1500	0.70	0.86	0.82
cg12011299	4	100065546	ADH4	TSS200	0.40	0.29	0.62
cg05635388	4	122721892	EXOSC9;EXOSC9	TSS1500;TSS1500	0.62	0.60	0.39
cg04096619	5	9547595	SNORD123;SEMA5A	TSS1500;TSS1500	0.81	0.93	0.86
cg06961054	5	56204405	SETD9;SETD9	TSS1500;TSS1500	0.53	0.24	0.33
cg06795995	5	56204613	SETD9;SETD9	TSS1500;TSS1500	0.42	0.19	0.24
cg25340688	5	135416398	MIR886	TSS200	0.49	0.53	0.45
cg03395511	6	291903	DUSP22	TSS200	0.32	0.52	0.26
cg13824270	6	4020946	PRPF4B	TSS1500	0.53	0.24	0.26
cg00944873	6	24646780	KIAA0319;KIAA0319;KIAA0319; KIAA0319;KIAA0319	TSS1500;TSS1500;TSS1500;TSS1500; TSS1500	0.33	0.40	0.36
cg07792871	6	29942706	HCG9	TSS200	0.31	0.26	0.35
cg17857094	6	30907280	DPCR1	TSS1500	0.69	0.42	0.66
cg05030953	6	31241000	HLA-C	TSS1500	0.31	0.11	0.57
cg03849834	6	41195891	TREML4	TSS200	0.81	0.40	0.79
cg03558010	6	46890220	GPR116;GPR116	TSS1500;5'UTR	0.77	0.79	0.93
cg02872426	6	110736772	DDO;DDO	TSS200;TSS200	0.33	0.25	0.88
cg07164639	6	110736958	DDO;DDO	TSS1500;TSS1500	0.24	0.27	0.76
cg21309351	6	138540608	KIAA1244;PBOV1	Body;TSS1500	0.78	0.81	0.89
cg14593639	6	142622028	ADGRG6;ADGRG6;ADGRG6;ADGRG6	TSS1500;TSS1500;TSS1500;TSS1500	0.47	0.54	0.71
cg05155812	7	855012	SUN1;SUN1;SUN1;SUN1	TSS1500;TSS1500;TSS1500;TSS200	0.59	0.66	0.59
cg08776296	7	134856544	C7orf49;C7orf49;C7orf49;C7orf49; C7orf49;C7orf49;C7orf49	TSS1500;TSS1500;TSS1500;TSS1500; TSS1500;TSS1500;TSS1500	0.61	0.42	0.77
cg00795791	7	135346062	PL-5283	TSS1500	0.63	0.98	0.78
cg17960959	7	135346502	C7orf73	TSS1500	0.53	0.75	0.57
cg21537187	7	135662562	MTPN;LUZP6	TSS1500;TSS1500	0.68	0.19	0.71
cg09293560	7	150068240	REPIN1;REPIN1;REPIN1;REPIN1	TSS200;5'UTR;Body;5'UTR	0.59	0.77	0.64
cg07547279	7	151433873	PRKAG2;PRKAG2;PRKAG2	TSS1500;Body;Body	0.61	0.93	0.50
cg20877230	8	6876684	DEFA3;DEFA1;DEFA1B	TSS1500;TSS1500;TSS1500	0.48	0.57	0.49
cg20223677	8	7332846	DEFB104B;DEFB104A	TSS1500;TSS1500	0.73	0.90	0.89
cg20934259	8	11997366	USP17L2;FAM66D	TSS1500;Body	0.69	0.88	0.78
cg03983883	8	79577618	ZC2HC1A	TSS1500	0.32	0.25	0.23
cg04046119	8	107460025	OXR1;OXR1;OXR1	TSS200;Body;Body	0.88	0.51	0.39
cg10596483	8	143751796	JRK;JRK	TSS1500;TSS1500	0.21	0.19	0.22
cg03249723	9	98880057	LOC158434	TSS1500	0.35	0.49	0.38
cg21717724	9	123604514	PSMD5;LOC253039	Body;TSS1500	0.66	0.70	0.40
cg04622888	9	124990010	LHX6;LHX6;LHX6;LHX6	TSS200;Body;Body;Body	0.57	0.94	0.75
cg13523132	9	139638566	LCN6;LCN10	3'UTR;TSS1500	0.85	0.82	0.77
cg08713344	10	3183772	PITRM1-AS1;PITRM1;PITRM1;PITRM1	TSS200;Body;Body;Body	0.66	0.91	0.79
cg10171609	10	5405573	UCN3	TSS1500	0.87	0.94	0.96
cg10379346	10	123355239	FGFR2;FGFR2;FGFR2;FGFR2;FGFR2; FGFR2;FGFR2;FGFR2	5'UTR;5'UTR;5'UTR;5'UTR;5'UTR; 5'UTR;TSS1500;Body	0.46	0.90	0.51
cg06791446	10	123355268	FGFR2;FGFR2;FGFR2;FGFR2;FGFR2; FGFR2;FGFR2	5'UTR;5'UTR;5'UTR;5'UTR;TSS1500; 5'UTR;5'UTR	0.51	0.87	0.54
cg25460273	10	129704427	PTPRE	TSS1500	0.50	0.78	0.62
cg18493115	11	1643842	HCCA2;KRTAP5-4	Body;TSS1500	0.82	0.97	0.95
cg07243930	11	3647365	TRPC2	TSS1500	0.68	0.32	0.68
cg15570860	11	8986840	TMEM9B;TMEM9B;TMEM9B;TMEM9B-AS1	TSS1500;TSS1500;TSS1500;Body	0.70	1.00	0.74
cg23722437	11	13983009	SPON1	TSS1500	0.65	0.89	0.73
cg23284931	11	13983273	SPON1	TSS1500	0.51	0.88	0.69
cg07093428	11	18433500	LDHC;LDHC	TSS1500;TSS1500	0.76	0.89	0.73
cg19767548	11	18433554	LDHC;LDHC	TSS1500;TSS1500	0.84	0.93	0.74
cg14332815	11	18433564	LDHC;LDHC	TSS1500;TSS1500	0.78	0.86	0.63
cg11821245	11	18433683	LDHC;LDHC	TSS200;TSS200	0.56	0.54	0.41
cg07469075	11	35548139	PAMR1;PAMR1;PAMR1;PAMR1	TSS1500;TSS1500;TSS1500;5'UTR	0.36	0.36	0.54
cg01578633	11	57159066	PRG2;PRG2;PRG2;PRG2	TSS1500;TSS1500;TSS1500;TSS1500	0.39	0.43	0.64
cg15971518	11	57159174	PRG2	TSS1500	0.28	0.14	0.51
cg23304078	12	739312	LOC100049716;NINJ2;NINJ2	TSS1500;Body;5'UTR	0.59	0.42	0.56
cg05578102	12	739986	LOC100049716;NINJ2;NINJ2	TSS200;Body;5'UTR	0.39	0.07	0.37
cg20927656	12	7863229	DPPA3	TSS1500	0.52	0.35	0.64
cg01120761	12	7903170	CLEC4C;CLEC4C	TSS1500;TSS1500	0.79	0.47	0.95
cg15411736	12	9886905	CLECL1	TSS1500	0.80	0.93	0.76
cg04531182	12	10563981	KLRC4-KLRK1	TSS1500	0.36	0.87	0.20
cg08041188	12	10564015	KLRC4-KLRK1	TSS1500	0.40	0.92	0.25
cg22221831	12	15039397	MGP	TSS1500	0.41	0.62	0.83

cg11180750	12	21283013	SLCO1B1	TSS1500	0.34	0.39	0.84
cg02656474	12	22198837	CMAS	TSS1500	0.29	0.09	0.35
cg03842440	12	41831532	PDZRN4;PDZRN4	TSS200;Body	0.60	0.30	0.80
cg05788368	12	110506138	C12orf76	TSS1500	0.62	0.62	0.81
cg13861644	12	130822286	PIWIL1	TSS1500	0.66	0.76	0.44
cg27630820	12	130822294	PIWIL1;PIWIL1	TSS200;TSS200	0.58	0.82	0.45
cg19272349	13	37681255	CSNK1A1L	TSS1500	0.66	0.71	0.61
cg04306507	14	55594613	LGALS3	TSS1500	0.42	0.45	0.70
cg26251192	14	74003199	ACOT1;HEATR4;HEATR4	TSS1500;5'UTR;5'UTR	0.57	0.59	0.58
cg18561199	14	95027379	SERPINA4;SERPINA4;SERPINA4	TSS1500;TSS1500;TSS1500	0.32	0.37	0.45
cg03012280	15	41098255	ZFYVE19;DNAJC17	TSS1500;Body	0.61	0.57	0.70
cg17395184	15	42750462	ZFP106	TSS1500	0.81	0.82	0.64
cg03433313	16	819064	MIR662	TSS1500	0.78	0.91	0.62
cg08624915	16	31538718	AHSP	TSS1500	0.73	0.40	0.72
cg26624021	16	56995739	CETP	TSS200	0.40	0.68	0.88
cg09889350	16	56995813	CETP	TSS200	0.33	0.55	0.84
cg17107388	16	58533766	NDRG4;NDRG4;NDRG4;NDRG4; NDRG4;NDRG4;NDRG4;NDRG4	TSS1500;TSS1500;TSS1500;TSS1500; TSS1500;Body;Body;Body	0.66	0.38	0.30
cg22273830	17	1508471	SLC43A2;SLC43A2;SLC43A2	TSS200;Body;Body	0.30	0.56	0.26
cg24587835	17	5674234	LOC339166	TSS1500	0.29	0.10	0.35
cg13377102	17	7832764	KCNAB3	TSS200	0.88	0.66	0.31
cg13407335	17	7832852	KCNAB3	TSS200	0.86	0.63	0.22
cg16513459	17	7832932	KCNAB3	TSS200	0.83	0.57	0.20
cg01323777	17	7832943	KCNAB3	TSS200	0.88	0.64	0.19
cg27162435	17	7833163	KCNAB3	TSS1500	0.73	0.43	0.16
cg14918082	17	7833237	KCNAB3	TSS1500	0.75	0.46	0.14
cg05513408	17	39166655	KRTAP3-1	TSS1500	0.62	0.36	0.69
cg11440486	17	48585216	MYCBPAP	TSS1500	0.55	0.42	0.54
cg20111217	17	48585264	MYCBPAP	TSS1500	0.53	0.44	0.58
cg00901687	17	48585270	MYCBPAP	TSS1500	0.51	0.40	0.54
cg07442736	17	65040607	CACNG1	TSS200	0.90	0.34	0.92
cg01147067	17	78233766	RNF213;RNF213	TSS1500;TSS1500	0.58	0.27	0.84
cg02398342	17	80708632	TBCD;FN3K	TSS1500;3'UTR	0.53	0.36	0.41
cg10004653	18	713071	ENOSF1;ENOSF1;ENOSF1	TSS1500;TSS1500;TSS1500	0.54	0.28	0.33
cg07100532	18	713085	ENOSF1;ENOSF1;ENOSF1	TSS1500;TSS1500;TSS1500	0.66	0.37	0.42
cg25317025	18	47019823	RPL17;RPL17;RPL17;RPL17;RPL17; RPL17-C18orf32;RPL17;RPL17;RPL17	TSS1500;TSS1500;TSS1500;TSS1500; TSS1500;TSS1500;TSS1500;TSS1500; TSS1500	0.41	0.17	0.46
cg04547181	19	6721855	C3	TSS1500	0.47	0.70	0.43
cg14279361	19	6721955	C3	TSS1500	0.23	0.39	0.23
cg12768975	19	6721965	C3	TSS1500	0.24	0.42	0.21
cg16474696	19	13875014	MRI1;MRI1	TSS1500;TSS1500	0.24	0.44	0.22
cg25755428	19	13875111	MRI1;MRI1	TSS1500;TSS1500	0.34	0.67	0.34
cg19882830	19	21264948	ZNF714;ZNF714;ZNF714;ZNF714	TSS200;TSS200;TSS200;TSS200	0.21	0.50	0.12
cg18805164	19	36265700	SNX26	TSS1500	0.52	0.08	0.55
cg23489630	19	44645078	ZNF234;ZNF234	TSS1500;TSS1500	0.71	0.94	0.76
cg22459517	19	55587193	EPS8L1	TSS200	0.59	0.68	0.51
cg07461715	19	57989332	ZNF772;ZNF772	TSS1500;TSS1500	0.62	0.95	0.51
cg25325723	20	6104886	FERMT1	TSS1500	0.74	0.96	0.98
cg14752227	20	34000481	UQCC;UQCC	TSS1500;TSS1500	0.80	0.74	0.73
cg04305670	20	43937273	MATN4;MATN4;MATN4;RBPJL; RBPJL;RBPJL	TSS1500;TSS1500;TSS200;Body; Body;Body	0.59	0.78	0.74
cg18287711	20	62288918	RTEL1;RTEL1;RTEL1;RTEL1;RTEL1- TNFRSF6B	TSS1500;TSS1500;TSS1500;TSS1500; TSS1500	0.70	0.24	0.31
cg12690462	21	43822540	UBASH3A;UBASH3A;UBASH3A	TSS1500;TSS1500;TSS1500	0.67	0.79	0.42
cg10296238	21	47605174	C21orf56;C21orf56	TSS1500;TSS1500	0.30	0.05	0.19
cg11466708	22	23974816	C22orf43	TSS1500	0.70	0.86	0.56
cg24989447	22	31730238	PIK3IP1-AS1;PATZ1;PATZ1;PATZ1	TSS1500;Body;Body;Body	0.53	0.68	0.79
cg01124132	22	32599511	RFPL2;RFPL2;RFPL2	TSS200;5'UTR;TSS1500	0.48	0.23	0.16
cg27308932	22	32600139	RFPL2;RFPL2	5'UTR;TSS1500	0.49	0.46	0.21
cg05019187	22	32601185	RFPL2	TSS1500	0.56	0.34	0.34
cg08161306	22	47169227	TBC1D22A;TBC1D22A;TBC1D22A; TBC1D22A;TBC1D22A	TSS1500;5'UTR;Body;Body;Body	0.53	0.41	0.46

Table S5. Gene set enrichment analyses of KEEG pathway and GO cellular component terms associated with the 1,000 most differentially methylated probes among affected subjects heterozygous for the *HIST1H1E* frameshift mutations and controls.

GO term	Description GO term (Cellular Component)	FDR	Gene Symbol
GO:0098590	Plasma membrane region	5.69e-11	ABCG2;ADORA2A;ANXA2;ARHGEF18;BCR;C2CD5;CDH13;CPEB4;DISC1;DLGAP1;EHD2;EPS8L1; ERC1;EXOC1; FERMT1;ITGB2;KANK1;KCNC1;KCNC4;KCNJ10;KIFAP3;MLC1;MYO1D;NDRG4;NRCAM;NRP1;P2 RX1;PARD3B; PDE6B;PKD1L1;PLB1;PRR12;PTH1R;RGS14;SCN10A;SCRIB;SLC1A1;SLCO1B1;STK39;SYNE1;SY NJ2;TACSTD2;TANC1;ZFYVE19
GO:0045202	Synapse	5.69e-11	ABR;ADORA2A;APBB2;BCL11A;BCR;CDH13;CPEB4;CPT1C;CYFIP1;DISC1;DLGAP1;DOCK10; ERC1;FGFR2;HDAC4;ITSN1;KCNC1;KCNC4;KCNJ10;MAGI2;MDGA1;NCK2;NRCAM;NRP1; P2RX1;PDE4B;PHACTR1;PLCB1;PRR12;PTPRN2;RAB6B;RAP1A;RGS14;RPS6KB1;SCN10A;SCRI B;SDK1; SLC2A8;SYN3;SYNE1;SYNJ2;TANC1;UCN3
GO:0097458	Neuron part	7.07e-11	ADORA2A;APBB2;ARID1B;ASRGL1;BCL11A;BCR;BRSK2;CCSAP;CDH13;CNTN4;CPEB4;CPT1C; CROCC;CYFIP1;DISC1;DLGAP1;DOCK10;ERC1;FBXO31;ITSN1;KCNC1;KCNC4;KCNJ10; KCNN3;KIFAP3;LMTK2;MAG;MAGI2;MBP;MTPN;MYO1D;MYO3B;NCK2;NFASC;NRCAM;NRP1;P 2RX1; PDE4B;PDE6B;PRPH2;PRR12;PTPRN2;RAB6B;RAP1A;RGS14;RPS6KB1;RPTOR;SCN10A;SCRIB; SLC2A8; SYN3;SYNJ2;TANC1;TSHZ3;UCN3
GO:0042613	MHC class II protein complex	0.001	HLA-DPB1;HLA-DQB1;HLA-DQB2;HLA-DRB1;HLA-DRB5
GO:0033267	Axon part	0.001	ADORA2A;APBB2;BRSK2;CPEB4;CYFIP1;ITSN1;KCNC1;KCNC4;LMTK2;MAG;MBP; MYO1D;NFASC;NRCAM;NRP1;PTPRN2;SYNJ2;TANC1;TSHZ3;UCN3
GO:0044463	Cell projection part	0.001	ADORA2A;AGBL2;APBB2;BRSK2;C2CD5;CATSPER4;CCSAP;CPEB4;CPT1C;CROCC; CYFIP1;DISC1;DNAH9;DOCK10;DUSP22;EPS8L1;FERMT1;ITSN1;KANK1;KCNC1; KCNC4;KIFAP3;LMTK2;MAG;MAGI2;MBP;MYO1D;MYO3B;NDRG4;NEDD1;NFASC;NRCAM;NRP1 ; PDE4B;PDE6B;PKD1L1;PLB1;PRPH2;PTH1R;PTPRN2;RGS14;RPTOR;SYNJ2;TANC1;TSHZ3;UCN 3;WDR66
GO:0120038	Plasma membrane bounded cell projection part	0.001	ADORA2A;AGBL2;APBB2;BRSK2;C2CD5;CATSPER4;CCSAP;CPEB4;CPT1C;CROCC;CYFIP1;DISC1 ; DNAH9;DOCK10;DUSP22;EPS8L1;FERMT1;ITSN1;KANK1;KCNC1;KCNC4;KIFAP3;LMTK2;MAG; MAGI2; MBP;MYO1D;MYO3B;NDRG4;NEDD1;NFASC;NRCAM;NRP1;PDE4B;PDE6B;PKD1L1;PLB1;PRPH 2;PTH1R;PTPRN2;

			RGS14;RPTOR;SYNJ2;TANC1;TSHZ3;UCN3;WDR66
GO:0044304	Main axon	0.003	ADORA2A;KCNC1;MAG;MBP;MYO1D;NFASC;NRCAM;UCN3
GO:0042611	MHC protein complex	0.003	HLA-DPB1;HLA-DQB1;HLA-DQB2;HLA-DRB1;HLA-DRB5
GO:0030424	Axon	0.004	ADORA2A;APBB2;BRSK2;CCSAP;CNTN4;CPEB4;CPT1C;CYFIP1;ITSN1;KCNC1;KCNC4;LMTK2; MAG;MBP;MTPN;MYO1D;NFASC;NRCAM;NRP1;PTPRN2;SCN10A;SYNJ2;TANC1;TSHZ3;UCN3
PATHWAY: KEGG number	**Description**	**FDR**	**Gene Symbol**
hsa04514	Cell adhesion molecules (CAMs)	0.001	CDH4;HLA-A;HLA-C;HLA-DPB1;HLA-DQB1;HLA-DRB1;HLA-DRB5;ITGB2;MAG;NFASC;NRCAM;NRXN3;SELL
hsa04940	Type I diabetes mellitus	0.002	HLA-A;HLA-C;HLA-DPB1;HLA-DQB1;HLA-DRB1;HLA-DRB5;PTPRN2
hsa05330	Allograft rejection	0.008	HLA-A;HLA-C;HLA-DPB1;HLA-DQB1;HLA-DRB1;HLA-DRB5
hsa05332	Graft-versus-host disease	0.008	HLA-A;HLA-C;HLA-DPB1;HLA-DQB1;HLA-DRB1;HLA-DRB5
hsa05416	Viral myocarditis	0.008	HLA-A;HLA-C;HLA-DPB1;HLA-DQB1;HLA-DRB1;HLA-DRB5;ITGB2
hsa05310	Asthma	0.016	HLA-DPB1;HLA-DQB1;HLA-DRB1;HLA-DRB5;PRG2
hsa05320	Autoimmune thyroid disease	0.024	HLA-A;HLA-C;HLA-DPB1;HLA-DQB1;HLA-DRB1;HLA-DRB5
hsa05150	Staphylococcus aureus infection	0.026	C3;HLA-DPB1;HLA-DQB1;HLA-DRB1;HLA-DRB5;ITGB2
hsa04145	Phagosome	0.026	C3;COLEC11;COLEC12;HLA-A;HLA-C;HLA-DPB1;HLA-DQB1;HLA-DRB1;HLA-DRB5;ITGB2
hsa04650	Natural killer cell mediated cytotoxicity	0.031	HLA-A;HLA-C;IFNAR2;ITGB2;KLRC4-KLRK1;MICA;PPP3R1;SH2D1B;SH3BP2

GO, Gene Ontology; FDR, false discovery rate; KEGG, Kyoto Encyclopedia of Genes and Genomes.